Cell Biomaterials

Article

Fibrin hydrogels regulate human astrocyte state and neuronal reprogramming

Graphical abstract

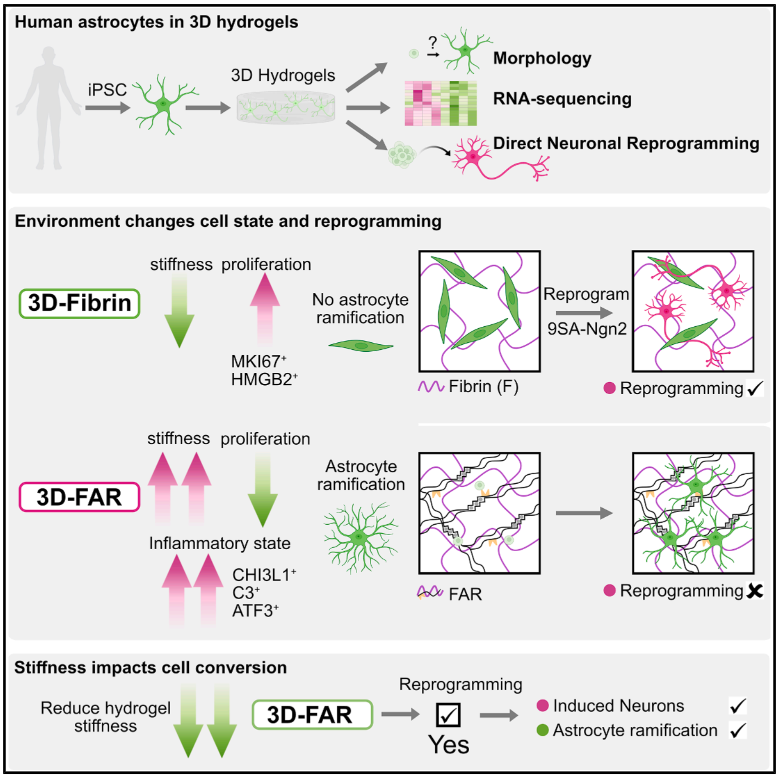

Highlights

- Transcriptomic analysis of human astrocytes in 3D-fibrin hydrogel and derivative
- Fibrin-alginate-RGD (3D-FAR) hydrogel increases astrocyte branching and reactive signatures
- 3D-fibrin hydrogels enable proliferation and migration of astrocytes
- Direct conversion of human iPSC-derived astrocytes into neurons in 3D-fibrin hydrogel

Authors

Thomas Distler, Katherina Konrad Daga, Martina Bürkle, Sebastián Vásquez-Sepúlveda, Kristian Franze, Magdalena Götz, Giacomo Masserdotti

Correspondence

magdalena.goetz@helmholtz-munich.de (M.G.), giacomo.masserdotti@helmholtz-munich.de (G.M.)

In brief

Dister et al. show that 3D-fibrin-derived hydrogels model injury-associated extracellular matrix effects on human astrocytes. Distinct fibrin-based matrices induce divergent reactive astrocyte states that differentially regulate astrocyte behavior and control the rate of Ngn2-mediated direct neuronal reprogramming.

Distler et al., 2026, Cell Biomaterials *2*, 100493
December 15, 2026
https://doi.org/10.1016/j.celbio.2026.100493

CellPress

Please cite this article in press as: Distler et al., Fibrin hydrogels regulate human astrocyte state and neuronal reprogramming, Cell Biomaterials (2026), https://doi.org/10.1016/j.celbio.2026.100493

Cell Biomaterials

CellPress
OPEN ACCESS

Article

Fibrin hydrogels regulate human astrocyte state and neuronal reprogramming

Thomas Distler,[1,2] Katherina Konrad Daga,[1] Martina Bürkle,[1,2] Sebastián Vásquez-Sepúlveda,[3,4] Kristian Franze,[3,4,5] Magdalena Götz,[1,2,6,7,*] and Giacomo Masserdotti[1,2,7,8,*]

[1]Biomedical Center Munich, Division of Physiological Genomics, LMU Munich, Martinsried, Germany
[2]Institute of Stem Cell Research, Helmholtz Center Munich, German Research Center for Environmental Health, Neuherberg, Germany
[3]Max-Planck-Zentrum für Physik und Medizin, Erlangen, Germany
[4]Medical Institute of Biophysics, Friedrich-Alexander-Universität Erlangen-Nürnberg, Erlangen, Germany
[5]Department of Physiology, Development and Neuroscience, University of Cambridge, Cambridge, UK
[6]Excellence Cluster of Systems Neurology (SYNERGY), Munich, Germany
[7]These authors contributed equally
[8]Lead contact
*Correspondence: magdalena.goetz@helmholtz-munich.de (M.G.), giacomo.masserdotti@helmholtz-munich.de (G.M.)
https://doi.org/10.1016/j.celbio.2026.100493

THE BIGGER PICTURE Neurons lost after brain injury are not naturally replaced in the adult mammalian brain, as neurogenesis is largely restricted to specialized niches. Direct neuronal reprogramming offers a promising strategy to regenerate neurons by converting resident non-neuronal cells, such as astrocytes located at the injury site, into functional neurons. However, it remains largely unknown how the three-dimensional injury microenvironment, enriched in extracellular matrix components such as fibrin after hemorrhage, affects this conversion process.

Here, we demonstrate that human induced pluripotent stem cell (hiPSC)-derived astrocytes can be directly converted into induced neurons (iNeurons) within 3D-fibrin hydrogels (3D-fibrin), which serve as an *in vitro* proxy for fibrin-rich brain injury environments. Increasing hydrogel stiffness, however, abolishes neuronal conversion, despite supporting astrocyte survival and the acquisition of highly ramified morphologies. Transcriptomic analysis reveals that this astrocyte state is associated with the activation of inflammatory gene programs. Importantly, reducing hydrogel stiffness partially restores astrocyte-to-neuron conversion in 3D-fibrin matrices.

Together, these findings reveal that astrocyte-to-neuron reprogramming is feasible in fibrin-rich 3D environments but is strongly constrained by pathological matrix stiffening. This work provides new insights into how injury-associated extracellular matrix properties influence cellular plasticity, with implications for brain injury modeling and regenerative strategies based on direct neuronal reprogramming.

SUMMARY

Astrocytes are key components in reactive gliosis after brain injury, yet defined *in vitro* models dissecting the influence of extracellular matrix components enriched after injury, such as fibrin, on human astrocyte behavior and function are still missing. Here, we use fibrinogen-derived fibrin and fibrin-alginate-RGD (FAR) 3D hydrogel substrates to examine their influence on human induced pluripotent stem cell (hiPSC)-derived astrocyte behavior and on their direct conversion into neurons. Astrocytes develop complex morphologies in 3D-FAR hydrogels, while they are more proliferative and migratory in 3D-fibrin hydrogels (3D-fibrin). Interestingly, gene expression analysis revealed different reactive states of astrocytes in 3D-fibrin and 3D-FAR, which persist over time. The highly inflammatory state and stiffness of 3D-FAR are largely incompatible with direct neuronal reprogramming, hampering the direct conversion even at early stages. Conversely, astrocytes in 3D-fibrin hydrogels can convert into neuronal cells, demonstrating a potent influence of how fibrin is presented on distinct astrocyte states, with great relevance for fate conversion.

Please cite this article in press as: Distler et al., Fibrin hydrogels regulate human astrocyte state and neuronal reprogramming, Cell Biomaterials (2026), https://doi.org/10.1016/j.celbio.2026.100493

INTRODUCTION

Astrocytes are the most abundant glial cell type in the mammalian central nervous system (CNS)[1,2] and play key roles in pathological conditions.[3–5] As such, they represent a promising target for therapeutic strategies by fostering their beneficial effects and reducing their adverse functions[6–8]: for example, the increased proliferation of juxtavascular astrocytes reduces the invasion of monocytes and scar formation,[9–11] while neurotoxic astrocytes hamper neuron function and survival.[12–14]

Blood-derived fibrinogen and its polymerized product fibrin directly affect border-forming and proliferating astrocytes in mouse models[15] but also regulate the expression and release of extracellular matrix (ECM) proteins[15]: this dual effect complicates investigating fibrinogen-specific effects from those of other components within the complex *in vivo* environment. Moreover, very little is still known about its influence on human astrocytes,[8] besides the general use of fibrin as a substrate in blood-brain barrier models, which support the growth of stem cell-derived human astrocytes.[16,17] Therefore, we set out to examine the impact of fibrin-rich 3D environments on human induced pluripotent stem cell (hiPSC)-derived astrocytes,[18,19] as fibrin is a key driver of lesion border-forming astrocytes.[15] We generated 3D-fibrin hydrogels (hereafter, 3D-fibrin), which reflect the soft nature of brain tissue[20] after acute injury, and compared them to hydrogels composed of fibrin and arginine-glycine-aspartic acid (RGD)-peptide-coupled alginate (hereafter, 3D-FAR), which show higher stiffness. This allowed us to identify profound differences in astrocyte states in 3D soft and stiff environments, with a remarkably potent influence on their capacity to be directly reprogrammed into neurons.

Even though proliferating astrocyte populations emerge after injury,[20] they fail to replace neurons that are lost after injury. However, proliferating astrocytes partially dedifferentiate, assuming hallmarks of neural stem cells (NSCs), and their neurogenic capacity can be revealed *in vitro* after removing them from the *in vivo* gliogenic environment[11] or by further manipulations, such as Notch deletion[21] or the expression of neurogenic fate determinants.[22] Excitingly, such proliferating astrocyte population was recently discovered in human pathologies.[23] However, little is known about which factors may impede the conversion of these, in principle, plastic astrocytes after brain injury. To tackle this question, we used the recently established direct reprogramming paradigm of hiPSC-derived astrocytes into neurons[19] and applied it to different 3D hydrogels (3D-FAR or 3D-fibrin). Interestingly, the former virtually completely interfered with the direct conversion into neurons, correlating with a highly inflammatory reactive state, as assessed by gene expression profile. Conversely, 3D-fibrin hydrogels allowed astrocytes to convert into neurons, showing the relevance and importance of modeling individual and combined ECM components in 3D for human astrocyte states and their response to fate conversion.

RESULTS

Human astrocytes acquire branching in 3D-FAR hydrogels

To test if a 3D environment influences hiPSC-derived astrocytes,[18,19,23] we first expanded the cells for 35 days in EGF/FGF-containing astrocyte medium (AM) and then embedded them in four different 3D hydrogels (Figures 1A and S1A): (1) soft sodium alginate at low concentration and molecular weight (0.5% w/v, 40 kDa), pre-functionalized with RGD peptide (GRGDSP, degree of substitution [DOS]: 0.375%, from manufacturer) as integrin ligands[24] at low density; (2) soft fibrin, offering different RGD sites by fibrinogen polymerization (e.g., Aα95–98 [RGDF],[25,26] Aα572–575 [RGDS],[25,26] and bovine: Aα252–254[27]); (3) Cultrex, derived from basement membrane (BME); and (4) FAR hydrogels, providing adhesion sites through both fibrin and alginate-RGD (Figure S1A). Seven days after seeding, astrocytes on 2D-poly-L-ornithine (PLO)-laminin (LAM)-coated glass coverslips (hereafter, 2D-POL), used as control, were flat (Figure S1A). Conversely, cells embedded in alginate-RGD for 7 days (days post embedding [dpe]) remained mainly round. Remarkably, in 3D-fibrin and Cultrex astrocytes showed an elongated morphology and network-like structure (Figure S1A), while they were more ramified in 3D-FAR hydrogels. This observation suggested that the fibrin and alginate-RGD in 3D-FAR have a synergistic rather than an additive effect. Therefore, we focused on the behavior of astrocytes embedded either in 3D-fibrin or in 3D-FAR hydrogels.

To get insights into the properties of the two hydrogels, we first analyzed their microstructure and stiffness, potentially influenced by the presence of Ca^{2+} ions used to crosslink alginate (Figure 1B). Performing multiphoton microscopy on 3D-fibrin and 3D-FAR hydrogels containing AF594-conjugated fibrinogen revealed a different microstructure (Figure 1C) and an increased porosity between fibrin fibers in 3D-FAR (Figures 1C and 1D), likely due to the presence of the alginate matrix. To assess the mechanical properties of the hydrogels, we performed atomic force microscopy (AFM) on 3D-fibrin and 3D-FAR hydrogels (Figure 1E) and also included Cultrex,[28,29] previously used for mouse astrocytes in 3D.[30] 3D-FAR hydrogels were 10× stiffer ($K_{eff} \sim 5{,}204$ Pa, $p < 0.0001$) than 3D-fibrin ($K_{eff} \sim 352$ Pa) or Cultrex BME gels ($K_{eff} \sim 438$ Pa), which are in the range of neonate-to-adult murine brain stiffness (~240–480 Pa[31]) and human gliotic tissue.[32] The stiffness of 3D-FAR hydrogels was in the range of human WHO grade IV glioblastoma brain tissue (~3–13.5 kPa[32]) and in accordance with previous observations that $CaCl_2$ can tune alginate stiffness,[33,34] thereby reinforcing other hydrogel matrices.[35] Importantly, the stiffness measured in 3D-fibrin and 3D-FAR gels was reproducible across different fibrinogen batches (Figure S1B).

Given the mechanical differences between 3D-fibrin and 3D-FAR hydrogels, we examined the behavior of green fluorescent protein (GFP)-labeled astrocytes by continuous live imaging after embedding them either in AF594-conjugated 3D-fibrin (Video S1) or AF594-conjugated 3D-FAR (Figures S1C–S1F; Video S2). While astrocytes could actively remodel 3D-fibrin hydrogel

Please cite this article in press as: Distler et al., Fibrin hydrogels regulate human astrocyte state and neuronal reprogramming, Cell Biomaterials (2026), https://doi.org/10.1016/j.celbio.2026.100493

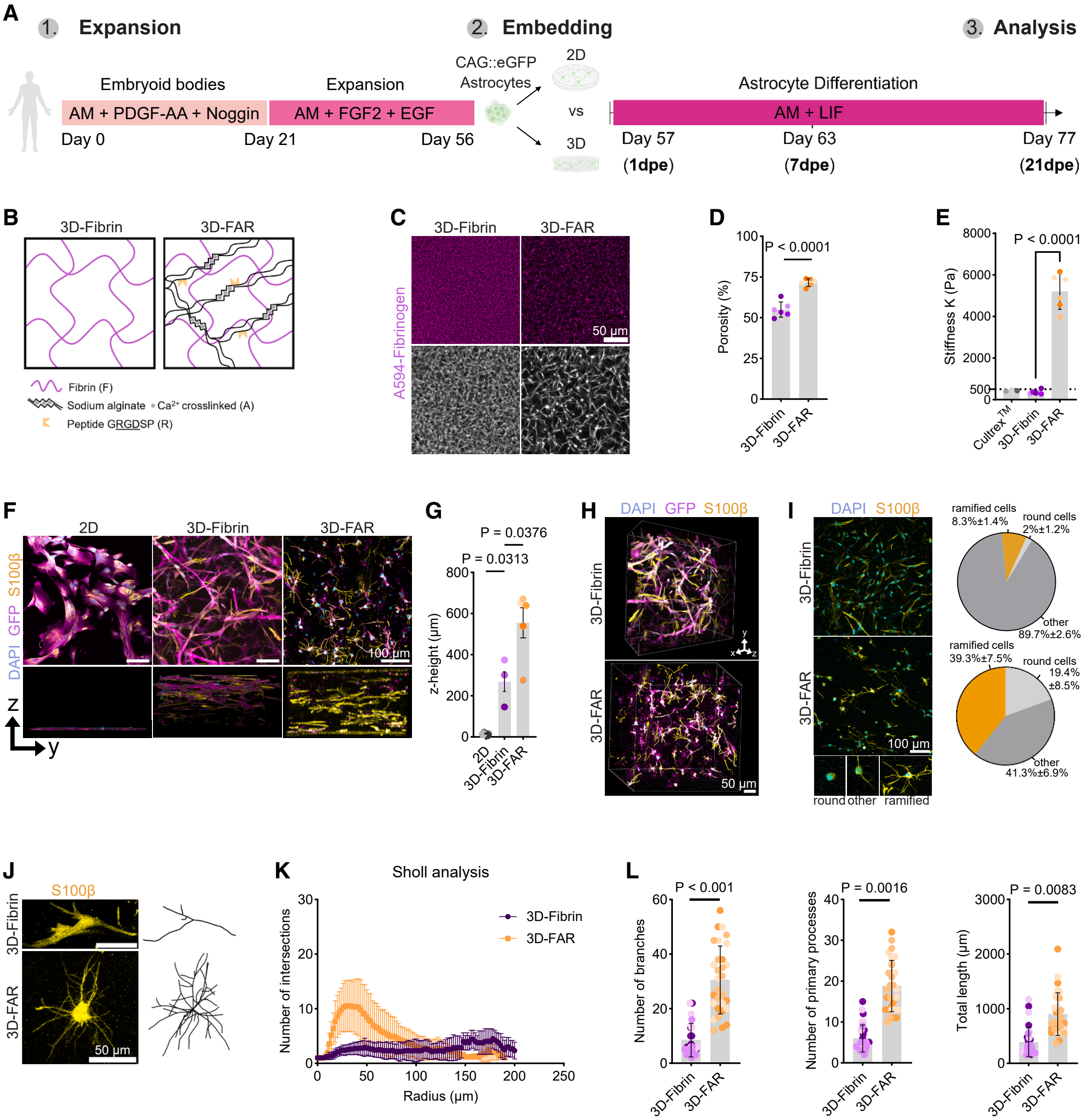

Figure 1. Characterization of hiPSC-derived astrocytes in 3D hydrogels

(A) Experimental design: iPSC-to-astrocyte differentiation protocol (left); embedding of astrocytes in 3D hydrogels or seeding on 2D-POL-coated coverslips (right).

(B) Scheme of 3D-fibrin and 3D-FAR hydrogels.

(C) Confocal microscopy images of 3D-fibrin and 3D-FAR microstructure by AF594 labeling of fibrinogen.

(D) Bar plot showing the percentage of microporosity, quantified as the volume between polymerized fibrin fibers in segmented images ($N = 3$; two technical gel replicates per N for fibrin and FAR; two-tailed t test, $p < 0.0001$).

(E) Bar plot showing the apparent elastic modulus (stiffness) K_{eff} of 3D-fibrin, 3D-FAR hydrogels, and Cultrex ($N = 3$ independent preparations and two hydrogel replicates per preparation [one technical replicate in case of Cultrex]; two-tailed t test, $p < 0.0001$).

(F) Examples of astrocytes on 2D-POL-coated coverslips or in 3D-fibrin and 3D-FAR hydrogels at 7 dpe.

(G) Graphs showing thickness (z-height) of hydrogels containing cells ($N \geq 4$; mean ± SEM; one-way ANOVA, $p < 0.05$).

(H) 3D image of astrocytes embedded in 3D-fibrin and 3D-FAR at 7 dpe.

(I) Pictures (left) showing the morphology of astrocytes embedded in 3D-fibrin or 3D-FAR: pie charts (right) illustrating the proportion of ramified astrocytes (S100β^+ cells with ≥three main processes) inside 3D-fibrin and 3D-FAR hydrogels at 7 dpe ($N = 3$ biological replicates; $n = 10$ cells analyzed per condition per biological replicate).

(J) Examples of astrocyte morphologies in 3D-fibrin or 3D-FAR hydrogels at 7 dpe.

(legend continued on next page)

Please cite this article in press as: Distler et al., Fibrin hydrogels regulate human astrocyte state and neuronal reprogramming, Cell Biomaterials (2026), https://doi.org/10.1016/j.celbio.2026.100493

(Video S1) and navigate through it (Video S3), 3D-FAR-embedded astrocytes were relatively immobile, rather extending and remodeling their processes (Video S2). We also observed cell division in both 3D-fibrin and 3D-FAR hydrogels (Videos S3 and S4), and cell death in 3D-FAR hydrogels (Video S4).

Overall, astrocytes cultured in both 3D substrates spread three-dimensionally (over ~250 μm of thickness in 3D-fibrin, up to ~500 μm in 3D-FAR; Figures 1F–1H; Videos S5, S6, and S7). Morphological analysis at 7 dpe supported the observations from continuous live imaging: ~39% of S100β$^+$ astrocytes inside 3D-FAR showed complex morphologies (equal to or more than three primary branches), while the rest were either less branched (~41%) or round (~19%) (Figure 1I). Conversely, in 3D-fibrin a small proportion of S100β$^+$ astrocytes showed a complex morphology (~8%), with almost 90% of the cells showing a simple (1–2 primary branches) or round (~2%) morphology. Noteworthy, Sholl analysis (Figures 1J–1L) revealed that ramified astrocytes in 3D-FAR are significantly more complex than 3D-fibrin-embedded counterparts (primary branches: 3D-FAR 20 ± 6, 3D-fibrin 8 ± 2, $p = 0.0016$; total number of branches: 3D-FAR 31 ± 11, 3D-fibrin 7 ± 2, $p < 0.001$; Figure 1L) and overall had longer processes (summed branch length: 3D-FAR ~900 μm, 3D-fibrin ~388 μm, $p = 0.0083$; Figures 1J–1L). Together, the data revealed that iPSC-derived astrocytes can be embedded in 3D hydrogels with different mechanical properties and microstructure, and this strongly affects the engagement of the cells with the substrates and their morphology.

Analysis of cell viability and proliferation of astrocytes in 3D-fibrin and 3D-FAR

At 7 dpe, more than 90% of GFP-labeled astrocytes in both 3D environments were S100β positive, but in 3D-FAR a much higher proportion of cells were positive for glial fibrillary acidic protein (GFAP), an astroglial marker usually upregulated upon reactive gliosis[12] (Figures 2A and 2B), thus suggesting a more reactive state in 3D-FAR hydrogels than in 3D-fibrin.

Next, we evaluated whether the concentration of Ca^{2+} (175 mM) used to crosslink alginate in 3D-FAR could contribute to the cell death observed in live imaging (Video S4), thus explaining the lower cell density found in this substrate (Videos S6 and S7). To this end, we crosslinked alginate-RGD inside 3D-FAR hydrogels with different Ca^{2+} concentrations (50, 100, and 175 mM) and, 4 days later, assessed cell viability (Figure 2C) using CalceinAM (green) and propidium iodide (PI, red) as live/dead markers, respectively (Figures 2C and 2D). Astrocytes were highly viable in 3D-fibrin (~90%; 1.6 mM Ca^{2+}, from AM) and showed a non-significant minor reduction in 3D-FAR at the concentration used for crosslinking (~80%, 175 mM Ca^{2+}; $p = 0.0659$; Figure 2E). To further evaluate the impact of Ca^{2+} on cell behavior, we assessed astrocyte morphology in 3D-fibrin hydrogels treated with the same Ca^{2+} concentration and time as in 3D-FAR: remarkably, we found a similar proportion of ramified cells in absence or presence of Ca^{2+} (3D-fibrin ~8%, 3D-fibrin + Ca^{2+}: ~5%, $p = 0.4392$; Figures S1G–S1K). Furthermore, whole hydrogel imaging showed morphologically ramified astrocytes throughout the 3D-FAR hydrogel, suggesting a homogeneous hydrogel microstructure and crosslinking throughout the hydrogel (Video S7). Together, our analyses indicated that a treatment of 10 min with Ca^{2+} required to crosslink alginate-RGD in 3D-FAR does not have a major impact on astrocyte viability or ramification, implying that the spatial microstructure and higher stiffness of 3D-FAR hydrogels may be instrumental to shape astrocyte morphology in such a 3D environment.

To analyze astrocyte proliferation on 2D and in 3D-fibrin/3D-FAR hydrogels, cells were treated with the DNA-base analog EdU twice, at the time of embedding and after 48 h, and analyzed 2 days later. Interestingly, astrocytes in 3D environments proliferated less than in 2D cultures, least in 3D-FAR (Figures 2G and 2H), resulting in a lower cell density in 3D-FAR already at 96 h (Figure 2I, $p = 0.0007$). We also tested the impact of fibrin on astrocyte behavior on 2D-coated glass: interestingly, astrocytes seeded on 2D-POL or on 2D-fibrin showed similar morphology (Figures S1L and S1M), proliferation, and density (Figures S1N–S1Q), thus suggesting that fibrin per se is not sufficient to explain the differences observed when cells are cultured in 3D-fibrin, but rather the 3D environment contributes to regulate cell proliferation.

Despite the lower proliferation and density, astrocytes embedded in 3D-FAR could be cultured in AM containing leukemia inhibitory factor (LIF) over several weeks (Figures 2J–2L), maintained the expression of GFAP, and their processes reached other cells in dense areas after 14 days (Figure 2K). Conversely, at the conditions tested (2 million cells/mL), 3D-fibrin hydrogels dissolved after 7 dpe. At higher density (5 million/mL), 3D-fibrin hydrogels could be cultured for more than 3 weeks, mostly due to a dense cell layer forming on top of the hydrogels, sealing it from erosion (see section "direct neuronal reprogramming in 3D hydrogels").

Taken together, our results suggest that a modest decrease in viability, combined with a pronounced reduction in proliferation, may account for the observed lower cell density in 3D-FAR compared with 3D-fibrin hydrogels after 96 h (Figure 2I).

RNA-seq reveals reactive astrocyte state in 3D-FAR and a cycling state in fibrin

3D vs. 2D

As astrocytes cultured on 2D-POL and 2D-fibrin showed similar phenotypes (Figures S1L–S1Q), we decided to investigate the impact of the 3D environments at the molecular level by comparing the transcriptome of astrocytes cultured for 7 days either on 2D-fibrin or in 3D-fibrin, thus maintaining the same substrate and reducing possible confounding factors (Figure S2A). Surprisingly, few genes were differentially expressed (Figure S2B; log$_2$fold change [log$_2$FC] > 1 and *padj* < 0.1; Table S1), possibly due to the heterogeneity of biological replicates (Figures S2C–S2F).

(K and L) Sholl analysis and morphology characterization of S100β$^+$ astrocytes grown in 3D-fibrin or 3D-FAR hydrogels at 7 dpe ($n = 30$ astrocytes per condition, from $N = 3$ biological experiments; different colors represent astrocytes from the same biological experiment). Data are shown as mean ± SD. Statistical analysis was performed on averages from each biological experiment using two-tailed *t* test).

Please cite this article in press as: Distler et al., Fibrin hydrogels regulate human astrocyte state and neuronal reprogramming, Cell Biomaterials (2026), https://doi.org/10.1016/j.celbio.2026.100493

Known astrocyte markers[19] were similarly expressed on 2D-fibrin and in 3D-fibrin (Figure S2D). As fibrin can interact with several components of the ECM, such as integrins[36,37] and collagen,[38] we wondered whether a different environment (2D vs. 3D) might affect their expression: indeed, some integrins and collagens were more expressed in a specific condition, although not significantly (e.g., *ITGA2*, *ITGA3*, *COL7A1*, *COL4A5*, and *COL4A6* in 2D and *ITGA9*, *ITGBL1*, *COL26A1*, and *COL19A1* in 3D; Figures S2E and S2F, respectively). Gene set enrichment analysis (GSEA) revealed the enrichment of genes associated with the secretory pathway in astrocytes embedded in 3D-fibrin (Figures S2G and S2H) and regulators of collagen in astrocytes on 2D-fibrin (Figures S2I and S2J; Table S2). Overall, transcriptomic comparison revealed a high degree of similarity between astrocytes cultured on 2D-fibrin and in 3D-fibrin, indicating that the substrate exerts a stronger influence than the dimensionality of the culture environment at transcriptomic level.

3D-FAR vs. 3D-fibrin

To evaluate the impact of different 3D substrates, we assessed the transcriptome of human astrocytes after 7 days in 3D-fibrin and 3D-FAR hydrogels (Figure 3A) and found significant changes in gene expression (125 more expressed in 3D-FAR, 154 in 3D-fibrin; $\log_2FC > 1$; $p$adj < 0.05; Figures 3B and 3C; Table S3). Gene Ontology (GO) analysis on genes more expressed in 3D-fibrin revealed an enrichment for genes associated with the regulation of the cell cycle (e.g., *MKI67*, *HMGB2*, *TOP2A*, *CENPE*, and *CENPF*; Figure 3D for biological process [BP], S3A, and S3B cellular compartment [CC] and molecular function [MF]; Tables S4, S5, and S6). Indeed, we detected a trend of more astrocytes ($S100\beta^+$ cells) positive for HMGB2[39] in 3D-fibrin than in 3D-FAR (Figures S3C and S3D), supporting the higher proliferation in 3D-fibrin than in 3D-FAR (Figure 2F). Conversely, genes expressed at higher levels in 3D-FAR were associated with response to inflammation (e.g., *C3*, *CHI3L1*, *CHI3L2*, *CD44*, *LCN2*, *LGALS3*, *LGALS1*, and *ATF3*; Figures 3B, 3C, and 3E; Table S7) and stress (Figures S3E and S3F; Tables S8 and S9), thus suggesting a strong reactive state. Of note, in 2D-POL cultures and in 3D-FAR hydrogels we found a similar high proportion of $S100\beta^+$ astrocytes positive for CHI3L1, a secreted protein impairing neurogenesis,[40] and much higher than in 3D-fibrin (Figures S3G and S3H), further supporting a distinct reactive state of astrocytes in 3D-FAR than in 3D-fibrin. As CHI3L1 is also part of human astrocyte maturity gene signatures,[41] we compared astrocytes in 3D-FAR and 3D-fibrin to genes associated with mature human astrocyte states[41] (Figure S3I). Interestingly, CHI3L1 was the only gene significantly ($p$adj < 0.05) more expressed in 3D-FAR compared with 3D-fibrin, thus indicating no overall difference in the maturation state between astrocytes cultured in the 2 different conditions. We then analyzed the expression of genes associated with different reactive states, either induced *in vitro* or *in vivo*. We found that 3D-FAR astrocytes express high levels of genes induced by interleukin (IL)-1β treatment in human astrocytes (Figure 3F),[18] markers for pan-astrocyte reactive state[42] (Figure S3J), and genes[42] more expressed in Alzheimer's patients' isolated astrocytes[43] (Figure S3K), though not significantly. Conversely, the transcriptome of 3D-fibrin astrocytes was characterized by the presence of several genes identified in a model of middle cerebral artery occlusion (MCAO) in a cluster of astrocytes with moderate infarction (Figure 3G; cluster AC_3[44]), thus suggesting a different type of reactive state. Remarkably, only a few integrins but not collagens were significantly differentially expressed between 3D-fibrin and 3D-FAR astrocytes (Figures S3L and S3M), suggesting a similar capability of the astrocytes to interact with the surrounding environments, which offered the same concentration of fibrin matrix (3 $mg.mL^{-1}$). As ECM-associated proteins were overall not changed, we looked at the expression of matrix metalloproteases (MMPs), which are capable of degrading a variety of ECM components[45]: only three MMPs implicated in neuroinflammation (*MMP3*, *MMP7*, and *MMP12*)[46,47] were slightly more enriched in 3D-FAR,[46,47] further suggesting 3D-FAR as a pro-inflammatory environment (Figure S3N). Moreover, given the different stiffness between 3D-fibrin and 3D-FAR, we wondered whether mechanosensitive coding genes could be differentially expressed: though some genes seemed to be more expressed in a specific condition (e.g., the transient receptor potential gene *TRVP4*, expressed in astrocytes[48,49] and important to regulate cell volume[50]), the biological variability reduced their statistical significance (Figure S3O).[48–51]

In summary, the comparison of 3D-fibrin vs. 3D-FAR astrocytes revealed significant differences in the proliferation capacity and reactive state, suggesting their use to investigate specific aspects of astrocyte biology and to use the 3D biomaterial environment to elicit different astrocyte phenotypes.

3D-FAR short- vs. long-term culture

To assess how prolonged culture influences astrocytes in 3D-FAR and evaluate possible changes in the inflammatory state, we compared the transcriptome of cells cultured in 3D-FAR for 7 or 21 dpe (Figures 3H and 3I). Remarkably, we found very few genes differentially expressed between the two time points (6 at 21 dpe; 7 at 7 dpe; $\log_2FC > 1$; $p$adj < 0.05; Figures 3H and 3I; Table S10), thus suggesting the maintenance of an inflammatory condition over weeks.[12] As such, the analysis of the transcriptome revealed that 3D-fibrin astrocytes are more proliferative, while 3D-FAR hydrogel maintains the cells in a reactive state over time.

Distinct effects of 3D-FAR and 3D-fibrin on direct astrocyte-to-neuron reprogramming

Our results suggested substantial differences between human astrocytes embedded in 3D-fibrin and 3D-FAR. 3D-fibrin is a softer and fibrin-rich hydrogel, and the embedded cells have a higher proliferation accompanied by a moderate reactive state, similar to an intracerebral hemorrhage condition where astrocytes resume proliferation[8,23] and brain ECM changes[15,51] with an enrichment in fibrin; 3D-FAR hydrogel is stiffer, and astrocytes in such hydrogel are less proliferative and show a stronger reactive state. Therefore, we wondered if and how direct reprogramming of human astrocytes to neurons might be influenced in these two very different 3D environments. To tackle this question, astrocytes were embedded in 3D-fibrin or 3D-FAR together with retroviral vectors encoding either a fluorescent protein alone (dsRed) or coupled to a phospho-resistant[52] form of Neurogenin 2 (9SA-Ngn2),[53–55] recently used to reprogram mouse[56] and

Please cite this article in press as: Distler et al., Fibrin hydrogels regulate human astrocyte state and neuronal reprogramming, Cell Biomaterials (2026), https://doi.org/10.1016/j.celbio.2026.100493

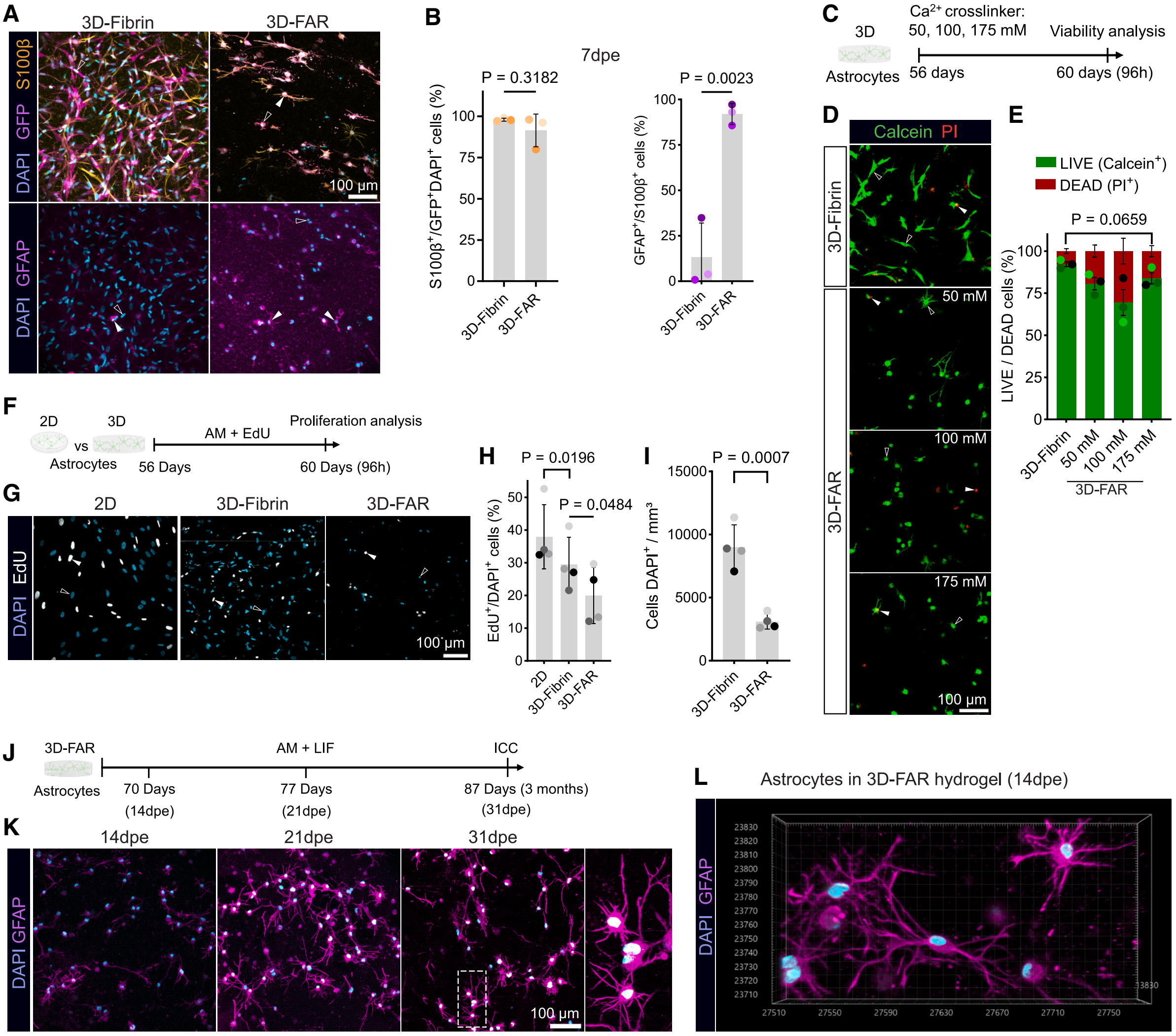

Figure 2. Analysis of astrocyte phenotypes in 3D-fibrin and 3D-FAR hydrogels

(A) Confocal microscopy images of S100β$^+$ and GFAP$^+$ astrocytes in 3D-fibrin or 3D-FAR hydrogels at 7 dpe. Scale bar, 100 μm.

(B) Bar plots showing the proportion of S100β$^+$ (left) and GFAP$^+$ (right) cells in 3D-fibrin and 3D-FAR hydrogels ($N = 3$; two-tailed *t* test; data shown as mean ± SD).

(C) Scheme of viability assay in astrocytes following the use of different concentrations of calcium chloride (50, 100, 175 mM) for crosslinking 3D-FAR hydrogel.

(D) Examples of astrocytes positive for Calcein$^+$ (alive cells, green) and PI$^+$ (dead cells, red). Scale bar, 100 μm.

(E) Bar plots showing the proportion of alive or dead cells after 4 days in either 3D-fibrin or 3D-FAR crosslinked with 175 mM $CaCl_2$ ($N = 3$; mean ± SEM; data point colors indicate different biological replicates; paired two-tailed *t* test).

(F and G) Scheme (F) and micrographs (G) of an EdU-incorporation assay to assess proliferation of astrocytes in 3D-fibrin, 3D-FAR, and on 2D-POL glass after 96 h. Scale bar, 100 μm.

(H and I) Bar plots showing the proportion of EdU$^+$ cells (H) and cell density (I) in 3D-fibrin and 3D-FAR gels ($N = 4$; mean ± SD; paired two-tailed *t* test).

(J–L) Scheme (J) and pictures of GFAP$^+$ astrocytes (K) cultured in 3D-FAR for different time points. Scale bar, 100 μm.

human astrocytes[19] (Figures 4A and 4B). 2D-POL cultures, transduced with either control or 9SA-Ngn2-encoding retrovirus, were used as controls (Figure 4B). To mitigate the impact of cell death during the conversion process,[19,22] we increased cell concentration to 5 mio.mL^{-1} in 3D (Figure 4A): this allowed culturing astrocytes not only in 3D-FAR (Figures 2F and 2G) but also in 3D-fibrin for up to 21 days (Figure 4).

Two days after transduction (2 dpt), ~33% of all cells were dsRed$^+$, independent of 2D or 3D conditions (Figures 4C and 4D), and almost all were S100β$^+$ (>97%, Figure 4E). After 21 dpt, very few astrocytes in 3D-FAR transduced with 9SA-Ngn2 were positive for the neuronal marker βIII-tubulin and showed at least one thin primary process, indicative of a neuronal morphology (~6%, Figures 4F and 4G). Conversely, both 2D and 3D-fibrin 9SA-Ngn2-transduced astrocytes converted into bona fide neuronal cells (~48%–61% of dsRed$^+$ cells were βIII-tubulin$^+$ cells and had a neuronal morphology; Figures 4F and 4G), reaching a density of ~1 × 10^3 βIII-tubulin$^+$-induced neuronal cells/mm^3 in 3D-fibrin (Figures 4H–4J). This was significantly higher than the density of induced neuronal cells

Please cite this article in press as: Distler et al., Fibrin hydrogels regulate human astrocyte state and neuronal reprogramming, Cell Biomaterials (2026), https://doi.org/10.1016/j.celbio.2026.100493

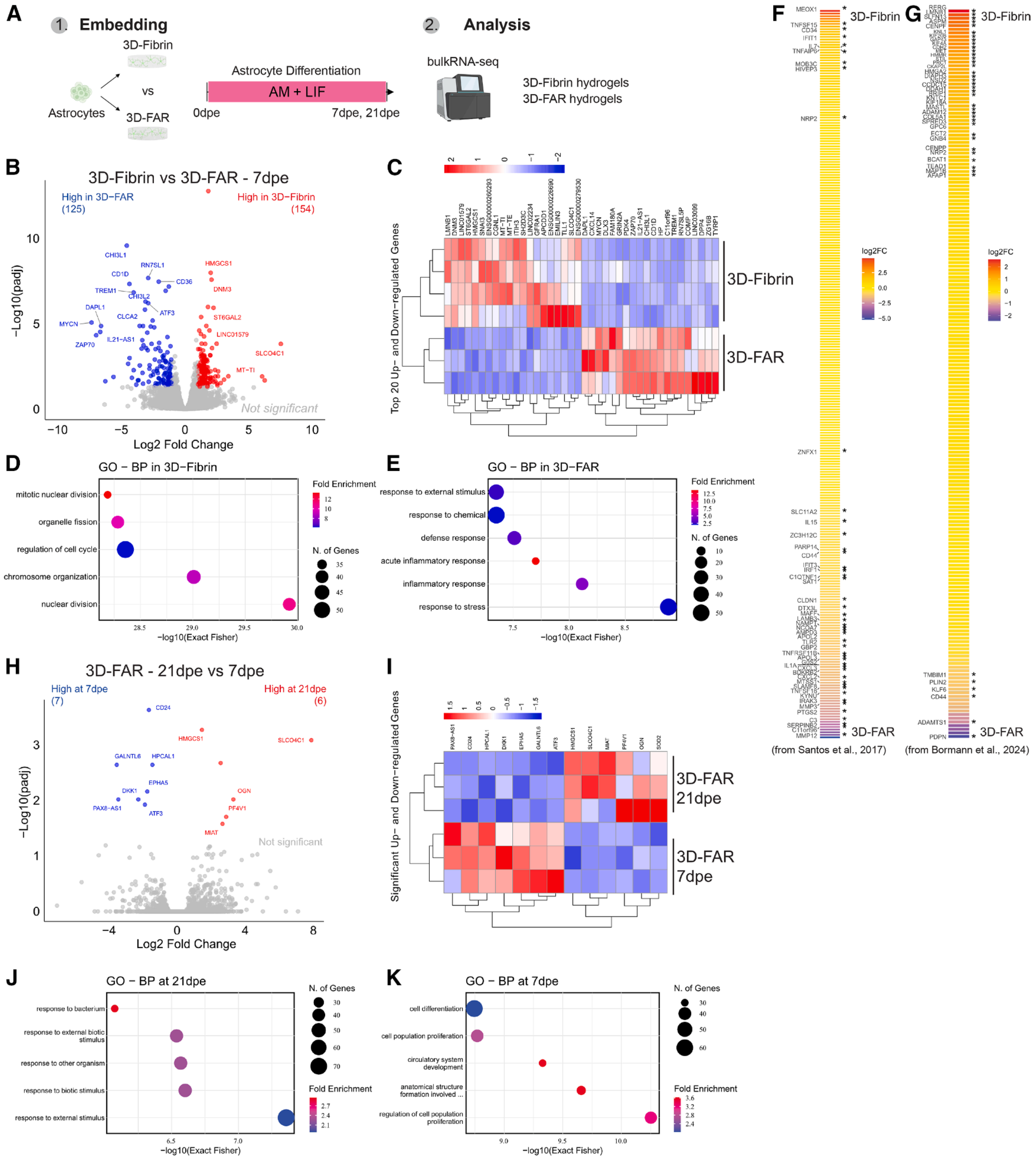

Figure 3. RNA-seq analysis of astrocytes embedded in 3D-fibrin and 3D-FAR hydrogels

(A) Experimental design. Astrocytes were cultured in different gels and collected for RNA-seq at different time points.

(B) Volcano plot showing DEGs (3D-fibrin, red; $\log_2FC > 1$, $p < 0.05$; 3D-FAR, blue; $\log_2FC < -1$, $padj < 0.05$). Names are indicated when $\log_2FC >$ abs(1) and $padj < 0.05$.

(C) Heatmap showing the top 40 genes more expressed by astrocytes in 3D-fibrin or 3D-FAR.

(D and E) GO analysis of BP from genes more expressed in 3D-fibrin ($\log_2FC > 1$, $padj < 0.05$) or in 3D-FAR ($\log_2FC < -1$; $padj < 0.05$).

(F and G) Heatmaps showing the $\log_2FC$ of genes induced in human astrocytes upon IL-1β treatment (Santos et al.,[18] left) and more expressed in astrocytes following MCAO injury (Bormann et al.,[44] right).

(H) Volcano plot showing DEGs in 3D-FAR at different time points (21 dpe, red; $\log_2FC > 1$, $padj < 0.05$; 7 dpe, blue; $\log_2FC < -1$, $padj < 0.05$). Names are indicated when log2FC > abs(1) and *padj* < 0.05.

(I) Heatmap showing the top 40 genes more expressed by astrocytes in 3D-FAR at 7 or 21 dpe.

Please cite this article in press as: Distler et al., Fibrin hydrogels regulate human astrocyte state and neuronal reprogramming, Cell Biomaterials (2026), https://doi.org/10.1016/j.celbio.2026.100493

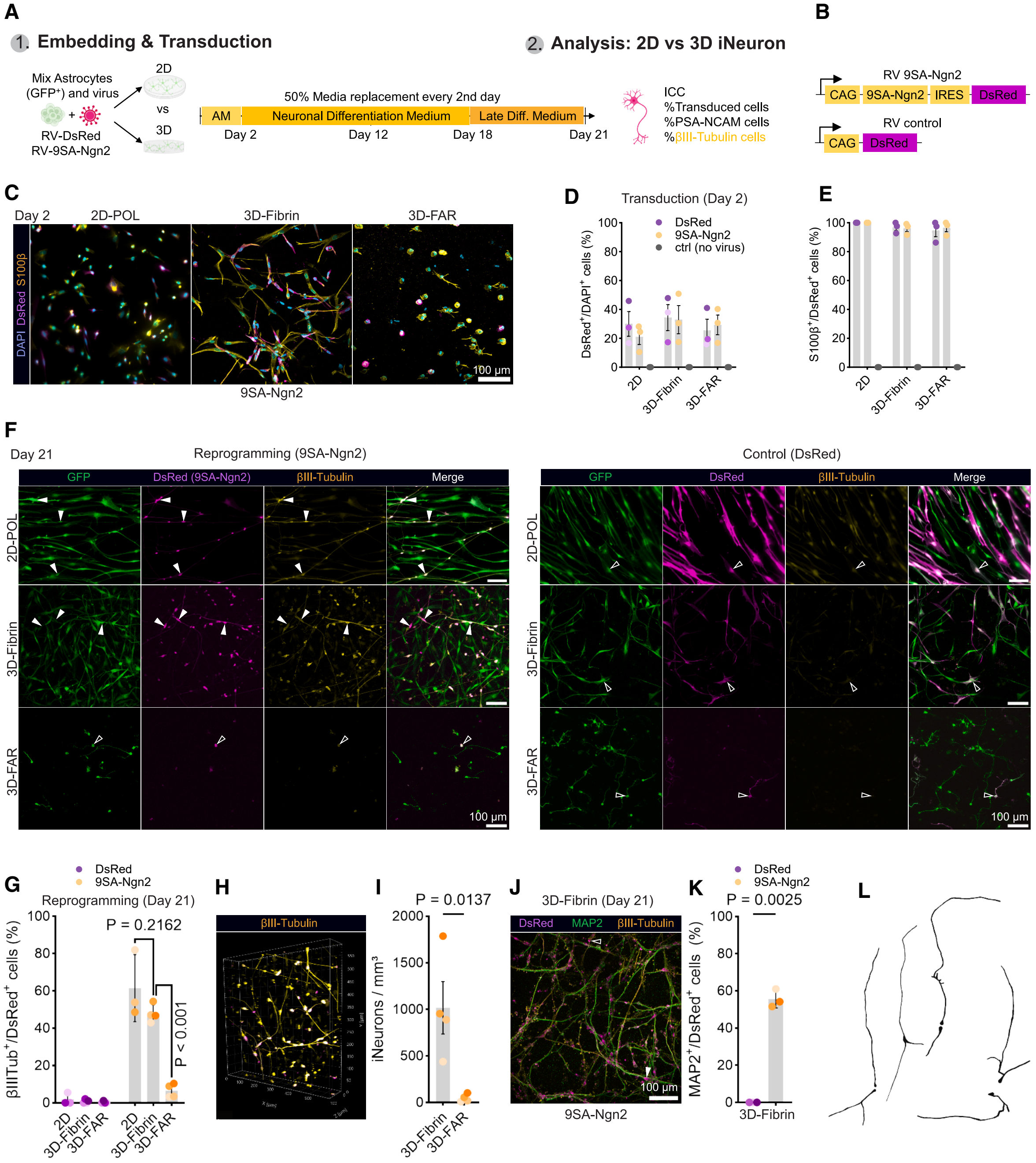

Figure 4. Direct neuronal reprogramming of astrocytes in 3D hydrogels

(A and B) Experimental design for direct neuronal reprogramming in 3D (A) and scheme of the retroviral vectors used for direct reprogramming (B).

(C–E) Confocal images of dsRed$^+$ viral transduced cells after 2 dpt (C), transduction efficiency for both viruses in 2D and 3D cultures (D, $N = 3$, mean ± SEM), and proportion of S100β$^+$ astrocytes transduced (E) ($N = 3$ [$N = 2$ for 2D-dsRed], mean ± SEM). Scale bar, 100 μm.

(F) z stack projections of pictures from 9SA-Ngn2-transduced astrocytes either on 2D-POL or in 3D hydrogel cultures (fibrin and 3D-FAR hydrogels) at 21 dpt. Scale bar, 100 μm.

(G) Bar plot showing the conversion rate at 21 dpt ($N = 3$–4; data shown as mean ± SD; colors indicate quantifications from independent experiments; one-way ANOVA).

(H) Micrograph of βIII-tubulin$^+$ cells in 3D-fibrin hydrogel at 21 dpt.

(I) Bar plot showing the density of iNeurons in 3D-fibrin and in 3D-FAR at 21 dpt ($N = 4$; data shown as mean ± SD; colors indicate data from independent biological experiments; two-tailed *t* test).

(J) Micrograph of dsRed$^+$MAP2$^+$ cells in 3D-fibrin hydrogel reprogrammed with 9SA-Ngn2 at 21 dpt.

(legend continued on next page)

Please cite this article in press as: Distler et al., Fibrin hydrogels regulate human astrocyte state and neuronal reprogramming, Cell Biomaterials (2026), https://doi.org/10.1016/j.celbio.2026.100493

(iNeurons) estimated in 3D-FAR (Figure 4I; $p = 0.0137$). Of note, at 21 dpt ∼55% of transduced cells in 3D-fibrin were also positive for the neuronal marker MAP2, indicating the acquisition of a more mature neuronal identity (Figures 4J and 4K; Video S8).

To check if 3D-FAR astrocytes could not be reprogrammed or may not survive until 21 dpt (Figure 2K), we analyzed the cultures undergoing direct conversion at 12 dpt (Figure S4). Interestingly, we found that PSA-NCAM (neuronal marker expressed by newborn neurons) was expressed by a high proportion of control- and 9SA-Ngn2 transduced astrocytes (Figures S4A–S4C; 40%–60% in controls; in 9SA-Ngn2 2D: ∼96%, 3D-fibrin: ∼99%, 3D-FAR: ∼82%), but at a significantly different level (Figure S4D; $p = 0.0100$). Remarkably, in 3D-FAR hydrogels a slightly lower proportion of PSA-NCAM^{+}βIII-tubulin^{+}/dsRed^{+} cells could be detected at 12 dpt (Figures 4A and 4E) and significantly lower compared with 2D culture ($p = 0.0184$). These transduced cells in 3D-FAR also appeared much smaller with much shorter processes compared with 3D-fibrin, thus suggesting that astrocytes in the 3D-FAR substrate were impaired in their fate conversion, possibly leading to cell death (Figures 4C and 4F). Consistent with this, we observed many round cells with pyknotic DAPI^{+} nuclei among dsRed^{+} cells in 3D-FAR, explaining the lower cell density of iNeurons in 3D-FAR at 21 dpt. In sharp contrast, a high proportion of 9SA-Ngn2-transduced cells seemed already converted into neuronal cells at 12 dpt in 3D-fibrin, as evident by their morphology (Figure S4A) and by the expression of βIII-tubulin^{+} (Figure S4E). Importantly, we did not observe reduced cell viability (Figures 5A–5C; CalceinAM^{+} cells >80%) among dsRed^{+} transduced cells (Figures S5A and S5B) at up to 96 h in the reprogramming paradigm, suggesting that the mitigated fate conversion or possibly compromised viability may occur at later stages.

Altogether, we concluded that hiPSC-derived astrocytes can be successfully reprogrammed into neuronal cells in 3D-fibrin hydrogels, where we observed uni- or bipolar elongated morphologies (Figure 4J). Direct neuronal conversion was compromised in stiff 3D-FAR hydrogels, where astrocytes showed a stronger inflammatory signature after 7 days (Figures 3C and 3K), highlighting the relevance of the 3D environment for direct neuronal reprogramming and the permissiveness of the 3D-fibrin environment to allow for the conversion of human astrocytes into neurons.

Stiffness reduction rescues direct reprogramming in 3D-FAR

As 3D-FAR elicited an inflammatory state in embedded astrocytes and offered a high stiffness environment exceeding physiological values of homeostatic brain tissue[57] (Figure 1E), we wondered which of the two parameters was responsible for the impaired reprogramming in 3D-FAR (Figure 5D). To test this, we first assessed the response of astrocytes to an inflammatory stimulus. 2D-POL astrocytes treated with IL-1β for 5 h (Figure S5C) showed a significant upregulation of genes associated with an acute inflammatory astrocyte state[18] (Figure S5E, *CXCL1*, *CXCL8* [*IL-8*], and *SOD2*) and the robust production of IL-6 both in 2D (Figure S5D; $p = 0.0216$) and 3D (Figure S5F; $p = 0.0013$) cultures. Interestingly, we also observed that astrocytes in 3D-FAR seem to secrete more IL-6 than those embedded in the 3D-fibrin (Figure S5F, FAR: ∼23.7 ± 5.8 pg.mL^{-1} [mean ± SD]; fibrin: ∼8.4 ± 4.5 pg.mL^{-1} [mean ± SD]), further evidence for a stronger reactive astrogliosis in 3D-FAR. Then, we reprogrammed astrocytes embedded in 3D-fibrin in control conditions (as Figure 4) or treated the cells with IL-1β for 5 h to induce an acute inflammatory state after cell embedding[18] (Figure 5E). Remarkably, the induction of a strong inflammatory state in 3D-fibrin astrocytes had no effect on their direct conversion, as we observed a similar proportion of dsRed^{+}βIII-tubulin^{+} cells with at least one thin primary process indicative of an early neuronal morphology (Figures 5F and 5G) and iNeuron density at 12 dpt (Figure 5H).

We then tested if the stiffness of the 3D substrate might be responsible for the observed low conversion rate in 3D-FAR.[58–60] To address this point, we engineered a 3D-FAR hydrogel of intermediate stiffness between 3D-fibrin and 3D-FAR (Figures S5G and S5H, K∼1.6 kPa, thereafter "3D-FAR-med"): in fact, by reducing the alginate content, the 3D-FAR-med substrate showed a stiffness similar to that of human gray and white matter brain tissue,[61] though the microstructure remained similar to 3D-FAR (Figures S5G–S5I). When embedded in 3D-FAR-med and cultured for 7 days, human astrocytes were highly ramified (Figure S5J), like those observed in 3D-FAR (Figure 1I). Remarkably, astrocytes embedded in 3D-FAR-med (Figure 5I) showed a significantly higher conversion rate (Figures 5J and 5K, $p = 0.0468$) and iNeuron density (Figure 5L, "stiff" vs. "med," $p = 0.0071$) compared with 3D-FAR. Indeed, the conversion in 3D-FAR-med was similar to 3D-fibrin astrocytes, although in the latter, iNeuron density seemed still higher (Figure 5L), thus suggesting the persistence of differences between 3D-fibrin and 3D-FAR-med. Furthermore, 3D-FAR-med iNeurons had longer processes than 3D-FAR iNeurons but not as long as in 3D-fibrin, while in 3D-FAR the direct reprogramming yielded mainly round cell morphologies (Figure 5J).

Importantly, our approach reduced the stiffness and density of the hydrogels simultaneously while keeping fibrin concentration constant: this suggests a combinatorial effect of both reduced stiffness and 3D environment density on the direct reprogramming and the growth of processes of iNeurons in 3D. Taken together, the results indicate that the mechanical properties of the 3D environment can significantly influence direct conversion of human astrocytes into iNeurons and their neuronal outgrowth in 3D.

DISCUSSION

Distinct astrocyte phenotype in 3D-fibrin vs. FAR

We show here that the choice of 3D substrate can drastically influence hiPSC-derived astrocyte morphology, phenotype, and

(K) Bar plot showing the percentage of dsRed^{+}MAP2^{+}/dsRed^{+} cells in the indicated conditions in 3D-fibrin hydrogels at 21 dpt ($N = 3$; data shown as mean ± SD; colors indicate data from independent biological experiments; $p < 0.0025$, paired two-tailed t test).

(L) Representative examples of iNeurons in 3D-fibrin (βIII-tubulin^{+}dsRed^{+}) with simple uni- or bi-polar elongated morphologies.

Please cite this article in press as: Distler et al., Fibrin hydrogels regulate human astrocyte state and neuronal reprogramming, Cell Biomaterials (2026), https://doi.org/10.1016/j.celbio.2026.100493

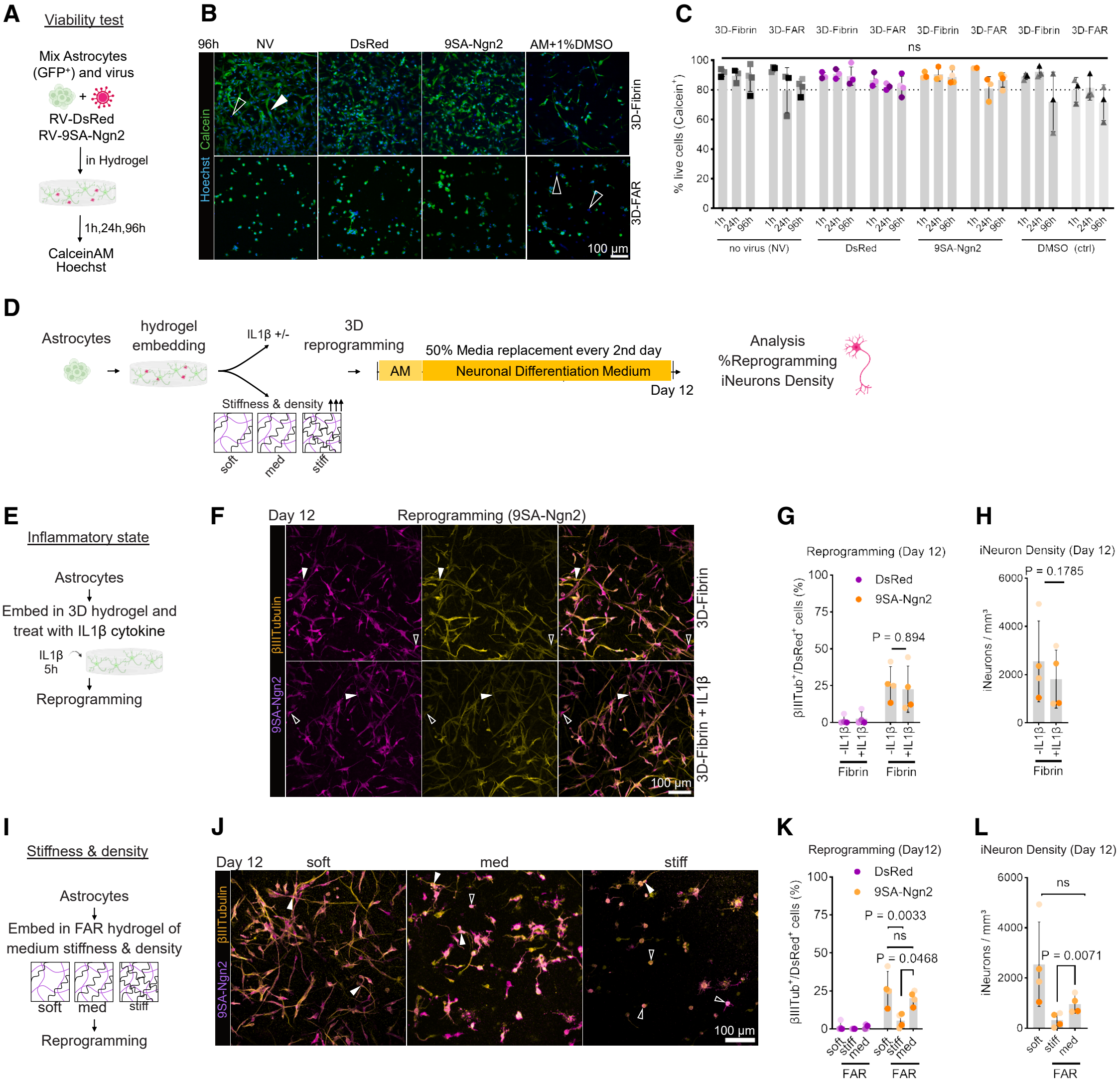

Figure 5. Direct reprogramming of astrocytes following inflammatory stimulation or stiffness changes

(A) Experimental design for viability assay in 3D-hydrogels during direct reprogramming.

(B) Micrographs showing Calcein^{+} astrocytes in 3D-fibrin and 3D-FAR hydrogels following dsRed- or 9SA-Ngn2 retroviral transduction; no virus (NV) control and AM + 1% (v/v) DMSO used as negative control.

(C) Quantification of Calcein^{+} cells after 1, 24, and 96 h post-transduction ($N = 3$–4 [$N = 2$ for 3D-FAR 9SA-Ngn2, 1 h], mean ± SD; ns, one-way ANOVA).

(D) Scheme of direct reprogramming astrocytes upon IL-1β treatment in 3D-fibrin or after embedding in hydrogels of different stiffness (3D-fibrin, soft; 3D-FAR, med, stiff).

(E) Experimental design for IL-1β-treated astrocyte reprogramming in 3D-fibrin.

(F) Micrographs showing cells undergoing neuronal conversion in 3D-fibrin or 3D-fibrin + IL-1β-treated (5 h) cells at 12 dpt. White filled arrowheads indicate βIII-tubulin^{+} dsRed^{+} cells; white empty arrowheads indicate βIII-tubulin^{-} dsRed^{+} cells.

(G) Bar plot showing the conversion rate at 12 dpt between ±IL-1β-treated conditions (one-way ANOVA, ns, $p = 0.894$, $N = 4$, mean ± SD).

(H) Bar plot showing the density of iNeurons (βIII-tubulin^{+}dsRed^{+} cells) per mm^{3} in 3D hydrogel ($N = 4$, mean ± SD one-way ANOVA; ns, $p = 0.1785$).

(I) Experimental design of direct reprogramming astrocytes in 3D-FAR hydrogels of different stiffness (med and stiff) vs. soft 3D-fibrin control hydrogels (soft).

(J) Example 3D images of βIII-tubulin^{+} dsRed^{+} iNeurons in soft, med, and stiff hydrogels (white filled arrowheads). White empty arrowheads indicate βIII-tubulin^{-} dsRed^{+} cells.

(K) Bar plot showing the conversion rate at 12 dpt of astrocytes embedded in hydrogels of different stiffness (soft, med, stiff) ($N = 4$, mean ± SD; one-way ANOVA, $p = 0.0468$ for 9SA-Ngn2-3D-FAR-med vs. 9SA-Ngn2-3D-FAR; $p = 0.6681$ for 9SA-Ngn2-3D-fibrin vs. 9SA-Ngn2-3D-FAR-med).

(L) Bar plot showing the density of iNeurons per mm^{3} in 3D hydrogels of different stiffness ($N = 4$, mean ± SD). Reducing hydrogel stiffness from stiff 3D-FAR to med 3D-FAR significantly increases the density of iNeurons in 3D hydrogels (one-way ANOVA, $p = 0.0071$).

Please cite this article in press as: Distler et al., Fibrin hydrogels regulate human astrocyte state and neuronal reprogramming, Cell Biomaterials (2026), https://doi.org/10.1016/j.celbio.2026.100493

reprogramming potential, as monitored by proliferation, migration, gene expression, and direct conversion experiments. Astrocytes embedded in 3D-fibrin maintained a rather simple morphology (3–5 primary branches), and this is associated with a proliferative state, as found by live imaging and gene and protein expression analysis. Conversely, astrocytes in 3D-FAR showed a rather complex morphology with up to 20 branches—similar to astrocytes grown in glia-enriched 3D cortical organoids with 10–15 primary branches[62]—which was surprisingly accompanied by a different, more inflammatory reactive transcriptional signature. Human astrocytes extended their processes along the 3D-fibrin structure (Video S1) and showed migratory behavior and degradation of the hydrogels, as shown before in fibrin[16,17,63] and other gel systems like pristine collagen[64] or derivatives. Conversely, hydrogel degradation and migration were mitigated by using collagen crosslinked with 4S-StarPEG[64] and in our 3D-FAR gel. This also allowed for longer cultures and was associated with a more complex astrocyte morphology and higher expression of genes either elicited by IL-1β treatment or associated with Alzheimer's disease (Figure 3F). Further studies will identify which aspects of these substrates are responsible for the differences observed in astrocyte phenotypes. As astrocytes in pure alginate-RGD (Figure S1) did not show pronounced branching and a low DOS with RGD peptides was provided on the alginate matrix in 3D-FAR (0.375% DOS; GRGDSP), it is unlikely that such a small increase in RGD concentration led to the observed changes. Rather, a synergistic effect of fibrin, alginate-RGD, stiffness, and change in microstructure shape astrocyte behavior (Figures 1C–1E). Interestingly, continuous live imaging in 3D-FAR showed that primary branches of astrocytes grow preferably along the AF594^{+} fibrin fibers (Video S2).

Noteworthy, the apparent elastic modulus K_{eff} measured via AFM in 3D-fibrin hydrogels (~300 Pa) was similar to that reported in human non-malignant gliotic tissue[32] (~10–180 Pa), while in 3D-FAR hydrogels K_{eff} was much higher (~5 kPa) and closer to values measured in human glioblastoma multiforme[32] (~3–13.5 kPa), indeed stiffer than physiological brain tissue (~1,000 Pa, fresh human tissue; or in bulk-tissue testing shear modulus G = 300–500 Pa, human brain tissue, *post mortem* time < 24 h[58]). It is important to note that stiffness is not sufficient to describe the complex mechanical properties of brain tissue,[65] and stiffness measurements differ profoundly depending on the technique used (e.g., AFM, magnetic resonance elastography [MRE], and rheology), across scales, loading modes (compression, tension, and shear[57]), speed, *post mortem* time, and tissue regions, such that a direct comparison to the *in vivo* situation is difficult. Yet overall, fibrin together with alginate-RGD peptides and much higher stiffness resulted in increased astrocyte branching at the expense of migration and proliferation.

The analysis of astrocyte proliferation and their transcriptome in 3D-fibrin and 3D-FAR revealed remarkable differences (Figures 2 and 3): cells in 3D-fibrin were more proliferative, similar to mouse astrocytes cultured on soft substrates (~300 Pa),[66] and showed a different reactive state compared with 3D-FAR. Indeed, a subset of astrocytes with this identity has been found in MCAO rats[44] and in lesions with intracerebral hemorrhage in mice[20,67] and men.[8,23] Conversely, the reactive signature of the astrocytes cultured in 3D-FAR hydrogels showed similarities to tumor-associated astrocytes,[41,68] human astrocytes treated with IL-1β,[18] and human Alzheimer's astrocytes (Figures 3F and S3K), as those conditions showed a higher expression of several inflammation-associated genes (e.g., *CHI3L1*, *CHI3L2*, *SLC7A11*, and *S100A4*).[41,43,68,69] Remarkably, the inflammatory signature of astrocytes in 3D-FAR persists over time, as only subtle differences could be detected at transcriptomic level between days 7 and 21 dpe (Figures 3H and 3I). 3D-FAR hydrogel shared several features with the peritumoral regions of human glioblastoma,[68] such as elevated stiffness[32] and pronounced reactive gliosis. This supports the use of such hydrogels to model a strongly adverse microenvironment.

Distinct astrocyte phenotypes differ profoundly in their capacity to convert into neurons

The functional relevance of these distinct astrocyte phenotypes elicited by the different 3D environments was demonstrated by their remarkable difference in neuronal reprogramming. Although 9SA-Ngn2-transduced astrocytes in 3D-FAR expressed the neuronal markers PSA-NCAM and βIII-tubulin at 12 dpt, many cells were round, indicative of an unhealthy state, and virtually no converted neurons could be detected under these conditions at 21 dpt. Thus, most of the astrocytes undergoing direct conversion might have reverted to an astrocyte identity or succumbed to cell death, a more likely possibility given the striking difference in cell density observed at 21 dpt (Figure 4F). Therefore, the 3D-FAR model is ideally suited to explore means to overcome the reprogramming blocks of highly reactive astrocytes with a chronic inflammatory signature and revert their phenotype to a healthier state. Conversely, astrocytes in 3D-fibrin readily reprogrammed into neuronal cells when transduced with the 9SA-Ngn2, with similar proportions to the classical 2D substrates described before.[19]

While it is likely that the persistent inflammatory signature in 3D-FAR contributes to the massively reduced conversion of astrocytes in stiff 3D-FAR hydrogels, our model shows that an acute inflammatory state elicited by IL-1β treatment in 3D-fibrin is not sufficient to prevent the direct reprogramming of human astrocytes (Figure 5). Conversely, we found that 3D stiffness substantially influences their 9SA-Ngn2-mediated direct conversion and iNeuron outgrowth: in fact, reducing the stiffness of 3D-FAR (Figures S5H and S5J) to a more physiological level[61] led to a significant increase in the reprogramming rate and the acquisition of a neuronal morphology, with thin and long processes. However, neuronal density and morphological complexity still hold behind those observed in 3D-fibrin, thus suggesting that either the presence of alginate or the stiffness (still double that of the 3D-fibrin hydrogel) contributes to the partial but not full rescue of the direct reprogramming phenotype, while astrocytes in 3D-fibrin were more proliferative and plastic toward direct conversion. Altogether, these observations shed light on the relevance of the stiffness and 3D microenvironment on the reprogramming process and have important implications for future direct reprogramming experiments of inflammatory-state astroglia in 3D, for reprogramming attempts in stiff grade IV glioblastoma environments,[32] or for the conversion of injury-associated

Please cite this article in press as: Distler et al., Fibrin hydrogels regulate human astrocyte state and neuronal reprogramming, Cell Biomaterials (2026), https://doi.org/10.1016/j.celbio.2026.100493

astrocytes[70] in soft ECM environments, such as after acute CNS stab wound injury.[71]

While the direct conversion of human fibroblasts into iNeurons in 3D has already been shown[72–74] and recently demonstrated for human glia spheroids,[75] we revealed for the first time how the specific ECM environment alters cell state and significantly contributes to shaping the direct conversion of human astrocytes into neuronal cells, which occurs in soft fibrin but not in a stiff 3D-FAR substrate.

An *in vivo* analogous astrocyte state exists, with astrocytes resuming proliferation after injury and partially dedifferentiating to an earlier progenitor fate.[11,23,76] Indeed, targeting viral vectors to this population allows efficient reprogramming in murine models of traumatic brain injury.[22] However, neuronal cells resulting from direct reprogramming in 3D-fibrin showed simple morphologies with hardly any branching and a single long primary process (Figure 4G). This, indeed, represents a novel model for future studies aimed at investigating the differentiation, maturation, and connectivity formation of newly generated neurons in 3D and identifying conditions (e.g., substrates, co-cultures, or co-factors) leading to the generation of fully functional 3D-embedded neuronal circuitry—likely being facilitated by increasing to higher cell density,[75] survival of converting cells, co-cultures, and higher viral titer.

Taken together, our work not only shows how different fibrin-containing substrates can elicit very distinct astrocyte states, revealing how this affects direct conversion into neurons, but also provides new model systems compatible with high-content screening for overcoming the inflammatory reactive astrocyte state resistant to reprogramming and optimizing reprogramming outcomes.

METHODS

hiPSC culture

iPSCs were cultured similarly to what was described before.[19] Briefly, hiPSCs were expanded on 6-well plates (Sarstedt) coated with Geltrex (LDEV-Free Reduced Growth Factor Basement Membrane Matrix, Thermo Fisher, A1413302; see Table S11 for reagents) in mTESR1 medium containing mTESR1 supplement (hiPSC medium). The medium was changed daily; passaging was performed via collagenase type IV (Stem Cell Technologies, 07909) treatment (37°C, 5–7 min). Collagenase was aspirated, and fresh medium was added to each well. Cells were collected using a cell scraper, followed by plating the cells on a new 6-well plate at a desired density (split ratios: 1:4 or 1:8). We used iPSC or generated transgenic iPSC constitutively expressing GFP, generated by Piggybac integration and selection.

Proliferating astrocyte differentiation from hiPSC

Human proliferating astrocytes (“astrocytes”) were generated as previously described.[19] In brief, hiPSCs were dissociated (collagenase IV) and cultured in suspension culture to form embryoid bodies. Next, cells were cultured for 24 h in hiPSC medium supplemented with Rock Inhibitor (10 mM, Y-27632, Stem Cell Technologies, 72304). On the next day, the medium was changed to AM (ScienCell, 1801) containing supplements (10 ng.mL^{-1} PDGF-AA, R&D Systems, 221-AA; 20 ng.mL^{-1} Noggin, Peprotech, 120-10C) in which the cells were cultured for 14 days, followed by another 7 days in AM containing just PDGFAA. On day 21, the embryoid bodies were dissociated with a pipette, and astrocytes were seeded on PLO- and LAM-coated petri dishes. Astrocytes were cultured in AM containing endothelial growth factor (10 ng.mL^{-1}, recombinant human EGF, Peprotech, AF-100-15) and fibroblast growth factor (10 ng.mL^{-1}, recombinant human FGF-basic, Peprotech, AF-100-18B) until day 35, with media changes every second day, and passaged using Accutase (StemPro Accutase, A11105-01) when reaching 80% confluency.

3D cell culture of human astrocytes in fibrin hydrogels

Fibrin hydrogels (final concentration: 3 mg.mL^{-1}) were prepared similarly to as described before[17] by combining equal amounts (v/v) of a solution A, containing fibrinogen (6 mg.mL^{-1}, from bovine plasma, Sigma Aldrich; 341573) and aprotinin (80 U.mL^{-1}, Roche, 10236632103) in 1× PBS, with a solution B containing thrombin in AM (4 U.mL^{-1}, Sigma Aldrich; T4648). Stock aliquots of fibrinogen, thrombin, and aprotinin were stored at −21°C and freshly thawed on the day of the experiment. Fibrinogen stock aliquots were thawed for 30 min at 37°C. Before hydrogel formation, aliquots were kept on ice prior to mixing solutions A and B. For culturing astrocytes in 3D-fibrin hydrogels, astrocytes (day 35) were detached using Accutase (3 mL, 7 min, per 10 cm petri dish) and counted using the direct trypan blue exclusion method using a Neubauer chamber (Carl Roth, T729.1). 400,000 cells were pelleted (300 rcf, 5 min) and redispersed in 100 μL of solution B (4 mio.mL^{-1}). Next, 50 μL of solution B was quickly mixed with 50 μL solution A, avoiding air bubbles, to ensure a homogeneous distribution of the cells. 12.5 μL of cell-containing hydrogel precursor was cast into d = 5 mm mini-wells, which were custom-prepared silicone wells covalently attached to glass coverslips (d = 12 mm) by plasma treatment.[77] Gels were allowed to polymerize at 22°C (room temperature [RT]) for 10 min. The final gels contained 3 mg.mL^{-1} fibrinogen, 40 μg.mL^{-1} aprotinin, 2 U.mL^{-1} thrombin, and 2 mio.mL^{-1} astrocytes. After polymerization, gels were covered with 1 mL of AM and transferred into an incubator for subsequent cell culture.

Culture in 3D alginate, Cultrex, and 3D-FAR hydrogels

Alginate

To culture astrocytes in 3D alginate-RGD hydrogels, low molecular weight sodium alginate pre-functionalized with RGD peptide by the manufacturer (Novatach; Cat# 4270101 VLVG, MW = 32,000 g.mol^{-1}, guluronic acid content >60%, 0.376% DOS, GRGDSP peptide) was used. Sodium alginate was dissolved in sterile 1× PBS to prepare a 2% (w/v) stock solution. Next, the cellular pellet (200,000 cells) was redispersed in alginate precursor (0.5% [w/v]), and 12.5 μL was cast into custom-made silicone mini-wells placed in 24-well plates (2 mio.mL^{-1}). To initiate crosslinking, the hydrogel precursor in the mini-well was covered using a dialysis membrane (washed in ddH$_2$O, cut into 9 × 9 mm squares, and pre-soaked in 175 mM CaCl$_2$ [prepared from Cat# 223506] solution). Hydrogels were covered with 1 mL of Ca^{2+} solution for 10 min to facilitate crosslinking of the alginate network. The initial covering using a dialysis membrane acted as a barrier

Please cite this article in press as: Distler et al., Fibrin hydrogels regulate human astrocyte state and neuronal reprogramming, Cell Biomaterials (2026), https://doi.org/10.1016/j.celbio.2026.100493

to avoid unwanted initial mixing of the $CaCl_2$ solution with the low-viscosity alginate precursor in the mini-well. After 10 min, Ca^{2+} solution was removed, the gels were washed once with 1× PBS for 1 min, and the cell-containing hydrogels were incubated in 1 mL of AM under standard incubation conditions (37°C, 5.0% CO_2).

Cultrex

Cultrex BME aliquots (Cultrex 3D BME, reduced growth factor, R&D Systems, 3445-005-01) were thawed on ice and pipetted for homogenization using cooled (4°C) pipette tips. Cell pellets were dispersed using the hydrogel precursor and pipetted (15 μL) inside a silicone mini-well, followed by homogeneous distribution via circular motion to prepare hydrogel discs. Cell-containing hydrogels were incubated for 30 min at 37°C in an incubator to facilitate hydrogel crosslinking.

3D-FAR

3D-FAR hydrogels were prepared similarly to fibrin hydrogels and without oxidation,[78] using a low molecular weight alginate (Novatach VLVG alginate stock; 2% [w/v], MW: 40,000 Da). Alginate-RGD was diluted in solution A components to achieve final concentrations of fibrinogen (6 $mg.mL^{-1}$), aprotinin (80 $U.mL^{-1}$), and 1% (w/v) alginate, in 1× PBS. A typical hydrogel solution contained 50 μL alginate (2% w/v), 36.4 μL 1× PBS, 1.6 μL aprotinin, and 12 μL fibrinogen (solution A: $V_{total} = 100$ μL, 1% [w/v] alginate, 6 $mg.mL^{-1}$ fibrinogen, and 80 $U.mL^{-1}$ aprotinin). Solution A was homogenized using a pipette. Hydrogel formation was triggered by mixing equal amounts of solution A with solution B (4 $U.mL^{-1}$ thrombin, in AM) containing the cells. The mixture was rapidly mixed by pipetting eight times, and the hydrogel mix (15 μL) was placed into the mini-wells. Final 3D-FAR gels contained the same amounts of fibrinogen, thrombin, and aprotinin as pure fibrin hydrogels, but additionally 0.5% (w/v) sodium alginate-RGD. Gels were allowed to gel for 10 min at RT. Then, hydrogels were covered with 175 mM $CaCl_2$ solution for another 10 min to crosslink the sodium alginate network inside the fibrin matrix, which resulted in interpenetrating network (IPN) hydrogels. Gels were washed for 1 min with 1× PBS and transferred into respective media (AM + LIF; or reprogramming medium).

For intermediate-stiffness 3D-FAR hydrogels (thereafter: "3D-FAR-med"), solution A contained 0.5% (w/v) alginate, leaving all other components constant, yielding a final concentration of 0.25% (w/v) alginate in intermediate-stiffness FAR hydrogels.

2D-POL-glass and 2D-fibrin cultures

To compare the effect of different 2D substrates on astrocyte morphology and proliferation, astrocytes (day 35) were seeded on glass coverslips coated with poly-L-ornithine (PLO) (20 $\mu g.mL^{-1}$, in ddH_2O, 16 h overnight at 37°C; Sigma Aldrich; P3655) and laminin (LAM) (10 $\mu g.mL^{-1}$ in 1× PBS, min. 16 h overnight at 37°C; Sigma Aldrich; L2020) to get 2D-POL-coated glass[19] and compared with astrocytes seeded on 2D-fibrin hydrogels. Briefly, 2D-fibrin hydrogels were cast into mini-wells by adding 12.5 μL of fibrin hydrogel (3 $mg.mL^{-1}$) distributed evenly in the wells and allowed to polymerize for 10 min at RT to create flat hydrogel discs. The hydrogels were prepared the same way as 3D-fibrin, but without embedding astrocytes (see "3D cell culture of human astrocytes in fibrin hydrogels"). Finally, astrocytes (35,000 in 1 mL AM + LIF per 24-well) were seeded either on top of 2D-POL-glass or on 2D-fibrin hydrogels, which were previously placed into 24-well plates, and cultured for 96 h or 7 days.

Mechanical testing by AFM

To assess the mechanical properties of Cultrex, 3D-fibrin, and 3D-FAR hydrogels, we performed AFM at 37°C immediately after hydrogel fabrication (~20 min for each gel; $N = 3$ for all conditions) from two independent batches of fibrinogen (Sigma Aldrich; 341573, #Lot1 3897584; #Lot2 4177330) in the case of 3D-fibrin and 3D-FAR. In detail, for Cultrex, three gels from individual preparations were measured. For 3D-fibrin and 3D-FAR hydrogels, a total of six gels were cast (three individual preparations for each #lot) for each type of gel. For intermediate-stiffness 3D-FAR hydrogels ("med"), five gels were measured and analyzed. AFM measurements were conducted on a JPK CellHesion 300 AFM (JPK Instruments), mounted to an upright setup with an Axio Zoom.V16 (Zeiss) microscope with a pco.edge 4.2 bi sCMOS camera. Tipless silicon cantilevers (Arrow-TL1, NanoWorld) with a custom-attached polystyrene bead as a probe (~37 μm diameter, microParticles) with a spring constant k (Arrow-TL1, NanoWorld) of 0.02–0.08 N/m, determined by the thermal noise method,[79] were selected. All samples were heated to 37°C using a PetriDishHeater (JPK Instruments) during all measurements. Bright-field images of the hydrogel surface before measurements were collected by a pco.edge 4.2 bi sCMOS camera connected to a Carl Zeiss Axio Zoom.V16 (Zeiss) microscope. Force-distance curves were recorded with a maximum indentation force of 5 nN and an approach speed of 10 $\mu m\ s^{-1}$ at a data rate of 2,000 Hz and analyzed with the JPKSPM Data Processing software (version 8.0.192). First, a baseline subtraction with correction for offset and tilt was conducted on the last 20%, followed by a correction for cantilever bending. Finally, the Sneddon model for a spherical indenter ($R = 18.64$ μm) was fit. To avoid any assumptions about the Poisson's ratio ν, ν was set to 0, yielding the reduced apparent elastic modulus K instead of the Young's elastic modulus E. Stiffness values are reported as K.

Microstructure analysis of fibrin and FAR hydrogels

The porosity and microstructure of 3D-fibrin and 3D-FAR hydrogels were imaged using a Leica Stellaris 8 FALCON system (20× and 40× objective). 3D-fibrin and 3D-FAR hydrogel fibers were visualized by substituting 1 μL of fibrinogen with 1 μL of Alexa Fluor 594-conjugated fibrinogen (Thermo Fisher, F13193) into solution A during hydrogel formation. The hydrogels were transferred to the microscope and imaged (field of view: 415 × 415 × 102 μm^3, voxel size: 0.4058 × 0.4058 × 2.0014 μm^3). The microstructure was analyzed from $N = 3$ independent hydrogel preparations. $AF594^+$ hydrogel fibers were segmented using threshold adjustment in ImageJ, followed by quantifying the area between $AF594^+$ hydrogel fibers.

Immunocytochemistry

Astrocytes cultured in 3D hydrogels were washed once using 1× PBS and fixed with 4% PFA (in 1× HBSS) for 10 min at RT. Samples were washed three times (10 min each) with 1× HBSS

Please cite this article in press as: Distler et al., Fibrin hydrogels regulate human astrocyte state and neuronal reprogramming, Cell Biomaterials (2026), https://doi.org/10.1016/j.celbio.2026.100493

followed by blocking and permeabilization for 1 h at RT using 3% BSA, 0.5% Triton X-100 in 1× HBSS. Next, 3D structures were immunostained with the following primary antibodies: mouse m1 anti-S100beta (Sigma, S2532, 1:1,000), rabbit anti-GFAP (Sigma, G9269, 1:300), rabbit anti-YKL-40/CHI3L1 (Abcam, ab77528, 1:300), rabbit anti-HMGB2 (Abcam, ab67282, 1:1,000), chicken anti-GFP (Aves Lab, 1020, 1:500), rabbit anti-RFP (Rockland, 600-401-379, 1:500), guinea pig anti-βIII-tubulin (Synaptic systems, 302–304, 1:200), mouse anti-polysialic acid-NCAM (Merck Millipore, MAB5324, 1:300), and anti-MAP2 (Sigma Aldrich, M4403, 1:500), in blocking solution, overnight at 4°C. The next day, samples were washed three times with 1× HBSS (15 min each) to remove the primary antibody solution and then incubated with secondary antibody (1:500) (for details, see summary of key experimental resources in supplementary figures) for 1.5 h at RT in the dark. Samples were washed three times with 1× HBSS (10 min each), and DAPI (1:1,000) was added to the second washing step to counterstain for nuclei when applicable.

Morphology analysis

The morphology of astrocytes in 3D-fibrin and 3D-FAR hydrogels was analyzed using segmentation, reconstruction, and Sholl analysis, as previously described.[62] Astrocytes were cultured for 7 days in 3D-fibrin or 3D-FAR hydrogels (2 mio.mL^{-1}) and stained for S100β to identify astrocytes. Astrocytes embedded in the hydrogels were imaged using a Leica SP8 Falcon system in two-photon excitation mode (lasers: Insight X3 DUAL, 1045, Spectra Physics, with tunable emission [680–1,300 nm]; pulse width <120 fs; second laser: 1,045 nm, pulse width <200 fs), equipped with a HC IRAPO L 25x/1.00 W motCORR (WD 2.6 mm) objective, with z-sectioning of 2 μm, 1,024 × 1,024 pixels, scan speed 400 Hz, and dwell time >1.5 μs. Single astrocytes were selected from the imaging z-stacks using Fiji[80] (ImageJ v1.5 4m), and astrocyte morphology was segmented and reconstructed by manual process tracing using neuTube[81] (v1.0z) to generate SWC files. Finally, astrocyte morphology was analyzed from SWC files by Sholl analysis (radius step size: 2 μm) using the simple neurite tracer[82] (SNT) plugin (v4.2.1). Parameters like total neurite length, number of branches, and number of primary branches were considered for analysis of astrocyte morphology ($n = 10$ cells per condition, $N = 3$ biological experiments, $n = 30$ cells in total for each condition, 3D-fibrin and 3D-FAR).

EdU proliferation study

EdU (10 mM) was added to AM at day 0 of cell seeding and embedding in the hydrogels, and a second EdU treatment was added after 48 h of incubation. Two days later, astrocytes were fixed and EdU detection was performed using the ClickiT plus EdU cell-proliferation kit (Thermo Fisher, C10640), which is based on a copper-catalyzed azide-alkyne cycloaddition (CuAAC) of an azide-fluorophore with the alkyne containing EdU. EdU was visualized by an azide-Alexa Fluor 647 probe supplied in the kit. All steps were performed according to the manufacturer's protocol. Nuclei were counterstained by DAPI (1:1,000) incubation for 15 min at the end of the ClickiT protocol, before the final washing with 1× HBSS. $N = 4$ biological experiments were performed. Astrocytes on 2D glass coated with PO+L served as control. EdU$^+$ cells were quantified from three overview images (598.05 × 598.05 × 50 μm^3) per condition per biological replicate. Cell quantification was performed via Fiji using the CellCounter (v3.0.0) plugin.

Viability analysis

To test the influence of different Ca^{2+} concentrations on astrocyte viability, we performed a LIVE/DEAD cell viability analysis. In brief, we used CalceinAM (4 μL.mL^{-1}, Thermo Fisher, C1430) and PI (1 μL.mL^{-1}, Sigma Aldrich, P4864) in 1× HBSS to indicate LIVE cells (CalceinAM conversion to fluorescent Calcein upon cell metabolism) and DEAD cells (PI incorporation by cell permeability), respectively. Cells were cultured in 3D-FAR hydrogels crosslinked with either 50, 100, or 175 mM $CaCl_2$. Astrocytes cultured in 3D-fibrin hydrogels (1.6 mM $CaCl_2$, from AM) served as control. After 96 h of astrocytes cultured in AM + LIF, the cells were incubated for 45 min at 37°C, 5% CO_2 in CalceinAM/PI solution, and directly transferred to a confocal microscope (Carl Zeiss LSM710 confocal) for imaging. Image stacks were recorded ($N = 4$ biological experiments, two technical replicates per condition, 485 × 485 × 50 μm^3). Alive cells (CalceinAM$^+$) and dead cells (PI$^+$) were quantified using Fiji.

Continuous live-cell imaging

To investigate the direct interaction of cells with the different 3D environments (3D-fibrin, 3D-FAR), we performed continuous live-cell imaging of CAG::eGFP hiPSC-derived astrocytes for the first 72 h of culture after embedding in the hydrogels. To visualize the hydrogel environment, we added 1 μL of AF594-fibrinogen during hydrogel formation. LIVE-cell imaging was performed in a humidified chamber (TokaiHit STXG) at 37°C, 5% CO_2, using a Leica Stellaris 8 FALCON system equipped with a 20× objective. Images were recorded every 30 min (field of view: 581 × 581 × 50 μm^3) to avoid phototoxicity. Images were processed for further analysis using Fiji (ImageJ). 3D animation and reconstruction of confocal and multiphoton images were performed using Imaris (Oxford Instruments, x64, v9.6.0).

Bulk RNA-seq

Astrocytes were cultured for 7 days (2D-fibrin, 3D-f) and for 7 and 21 days (3D-FAR) in the hydrogels and subjected to bulk RNA sequencing (RNA-seq) analysis. RNA was isolated using the Arcturus PicoPure RNA isolation kit (Thermo Fisher, KIT0204) following the manufacturer's instructions. Hydrogel discs containing the cells were scooped out from the mini-wells, homogenized in 100 μL of RNA extraction buffer in 500 μL Eppendorf tubes, briefly centrifuged, and incubated for 30 min at 42°C. RNA samples were stored at −80°C until the subsequent RNA purification step. After purification, RNA quality was determined using a 2100 BioAnalyzer (Agilent) and the RNA 6000 pico kit (Agilent Technologies, 5067-1513). RNAs with a sample RIN value ≥ 7.9 (mean RIN = 8.7 ± 0.6) were selected for mRNA sequencing (poly-A selected). RNA quantity was determined using the Qubit RNA High Sensitivity (HS) kit, and 10 ng of RNA (in 10.5 μL non-DEPC-treated H_2O) was pipetted into a Greiner Bio sapphire microplate 96-well (Greiner Bio-one, 652290). Library

Please cite this article in press as: Distler et al., Fibrin hydrogels regulate human astrocyte state and neuronal reprogramming, Cell Biomaterials (2026), https://doi.org/10.1016/j.celbio.2026.100493

preparation was performed using the SMART-seq mRNA LP kit (Takara, 634769) starting with 10 ng total RNA, following the kit's instructions. After a final QC, the libraries were sequenced in a paired-end mode (2 × 100 bases) in the NovaseqX+ sequencer (Illumina) with a depth of $\geq$30 million reads per sample. RNA-seq raw data processing was performed in Galaxy (see data and code availability). Reads were trimmed using Trimmomatic[83] (v0.4), and the transcriptome was aligned against the human genome hg38 (GRCh38) reference, version 32 (Ensembl 98),[84] using STAR aligner (v2.7.11b). We analyzed three biological replicates for 3D-FAR (7 and 21 dpe) and four biological replicates for 2D-fibrin and 3D-fibrin per condition.

Raw data are available at the following address: https://www.ebi.ac.uk/biostudies/studies/S-BSST2128.

Bioinformatic analysis of bulk RNA-seq data

Data analysis of bulk RNA-seq data was performed in R Studio (v2024.04.2). Count matrices were TPM normalized. Differentially expressed gene (DEG) analysis was conducted using DESeq2 (v1.44.0) analysis of the raw count matrix. Genes were considered differentially expressed with log$_2$FC change >1 (upregulated), or <−1 (downregulated) and $p$adj < 0.05 (or $p$adj < 0.1 for 3D-fibrin vs. 2D-fibrin comparison). GO analysis was performed using TopGo.[85] GSEA was performed using fgsea package.[86] Heatmaps of DEG data and comparison to different astrocyte scores[20,41,43] were plotted using the pheatmap package (v1.0.12). Volcano plots were generated using ggplot2.

Direct neuronal reprogramming in 3D hydrogels

To investigate the conversion of astrocytes into iNeurons, we reprogrammed astrocytes inside 3D-fibrin and 3D-FAR hydrogels by mixing cells, viral particles, and hydrogel in one step: astrocytes (10 mio.mL^{-1}) were redispersed in solution B (AM + thrombin) and mixed 50:50 with solution A containing fibrinogen, aprotinin, and virus (titer: $2.5 \times 10^{4–5}$ viral particles/35,000 cells in all conditions). In case of 3D-FAR, solution A contained sodium alginate-RGD as well (all in PBS; final cell concentration: 5 mio.mL^{-1}). The volume of PBS was adjusted so that the addition of virus did not alter the concentration of the final hydrogel components (final concentration: 3 mg.mL^{-1} fibrinogen; 25 μL hydrogel cast per mini-well). We used a retrovirus CAG-9SA-Neurog2-IRES-dsRedExpress2[19] (9SA-Ngn2) to express the phospho-resistant form of neurogenin 2, or retrovirus CAG-dsRedExpress2[87] as a control virus. Retrovirus vectors were produced,[19] titered[88] and used at a stock titer of 10^7–10^8 mL^{-1}. The reprogramming paradigm was similarly performed as described before[19]: astrocytes in 3D hydrogels and on 2D POL glass controls were cultured in neuronal differentiation media (DMEM/F12 + neurobasal media [1:1], supplemented with 1× PS, 1× B27, 1× N2, and 1× MEM non-essential amino acids [NEAAs]), which was supplemented with factors GDNF (2 ng/mL), CHIR99021 (2 mM), LDN-193189 (0.5 mM), LM-22A4 (2 mM), NT3 (10 ng/mL), SB-431542 (10 mM), db-cAMP (0.1 mg/mL), Noggin (50 ng/mL), and valproic acid sodium salt (VPA; 1 mM).[19,89] Every second day, half of the medium was replaced with fresh medium. Cultures undergoing direct reprogramming were maintained at 37°C, 5% O$_2$, 5% CO$_2$, in an incubator.[90,91] On day 18, neuronal differentiation media were supplemented with db-cAMP, GDNF, LM-22A5, and NT3.[19] Cells were fixed on day 21 (4% PFA, 10 min), washed (three times 1× HBSS, 10 min), and stored at 4°C until further use. Transduced cells were considered successfully converted neuronal cells when βIII-tubulin$^+$dsRed$^+$ cells showed at least one thin process indicative of a neuronal morphology. To assess early conversion, cells were cultured for 12 days, and early neuronal fate of transduced cells was quantified as PSA-NCAM$^+$βIII-tubulin$^+$dsRed$^+$ and PSA-NCAM$^+$/dsRed$^+$ cells. PSA-NCAM intensity of dsRed$^+$ cells was quantified by measuring the mean PSA-NCAM fluorescence intensity of single cells per condition (3D-FAR: 93; 3D-fibrin: 128; 2D: 103) using Fiji (ImageJ). Regions of interest (ROIs) on maximum intensity projections of single cells were manually drawn, or by thresholding when applicable, followed by subtraction of the average image background intensity from 3 × 100 μm^2 selections from individual images.

Astrocyte reprogramming in hydrogels of various stiffness and upon IL-1β stimulation

To test the effect of hydrogel stiffness on astrocyte conversion, direct neuronal reprogramming was performed in 3D-fibrin (soft), 3D-FAR (stiff), and an intermediate-stiffness FAR hydrogel (med), which contained 0.25% (w/v) alginate-RGD, leaving the fibrin concentration constant.

To test the effect of inflammatory cytokine treatment on astrocyte conversion in 3D, astrocytes embedded in 3D-fibrin were stimulated using IL-1β (10 ng.mL^{-1}) in AM for 5 h at 37°C, followed by medium change and the direct neuronal reprogramming paradigm in 3D. The efficiency of IL-1β treatment was confirmed by measuring the IL-6 secretion into the medium using an IL-6 ELISA (ProteinTec, KE00385) following the manufacturer's instructions and real time (RT)-qPCR (RNA isolation from cell pellets via Monarch Total RNA Miniprep Kit [BioLabs, #T2010S], cDNA synthesis via Maxima First Strand cDNA Synthesis Kit for RT-qPCR [TAKARA, #638.948], and final RT-qPCR: PowerUp SYBR Green Master Mix [Life Technologies] on a ROCHE LightCycler system). All preparations were performed according to the manufacturer's instructions. qPCR data are presented as the expression of each gene from triplicate values and processed via the ΔΔCt method using GAPDH as a housekeeping gene.

Statistical analysis

All experiments were performed with at least N = 3 biological replicates per condition. Image analysis was performed blinded using the "Blind Analysis Tools" file name encrypter toolbox (ZMBH Imaging Facility, University of Heidelberg) in ImageJ. All statistical tests are indicated in the presented figure captions. Statistical analysis was performed either using GraphPad Prism software (v10.4.1) or R (bulk RNA-seq data analysis; DESeq2). Pairwise comparisons of two conditions were performed using a paired Student's t test. Non-normally distributed data were analyzed using Welch's t test. Comparisons between more than two conditions were performed using one- or two-way ANOVA. For morphological analysis, statistical testing was performed on average values from the single cells measured in individual experiments (N = 3) and not on single-cell events.

RESOURCE AVAILABILITY

Lead contact

Further information and requests for resources and reagents should be directed to and will be fulfilled by the lead contact, Dr. Giacomo Masserdotti (giacomo.masserdotti@helmholtz-munich.de).

Materials availability

This study did not generate any new, unique reagents. Hydrogel materials were purchased from the respective vendors listed in the methods below. No chemically modifying syntheses of new materials were performed.

Data and code availability

- Data: RNA-seq data have been deposited at https://www.ebi.ac.uk/biostudies/studies/S-BSST2128 as fastq files (Database: S-BSST 2128) and are publicly available as of the date of publication.
- Code: standard Galaxy workflow for raw RNA-seq data processing (paired-end sequencing, MultiQC report) was used. The paper does not report original code. All the packages used for the analysis are indicated in the "methods" and "key resource" sections.
- Any additional information required to re-analyze the data reported in this paper is available from the lead contact upon request.

ACKNOWLEDGMENTS

We thank Dr. Andreas Thomae and Dr. Mariano Pisfil from the BMC Bioimaging facility for supporting two-photon microscopy and live-cell imaging and Dr. Madeleine Schmitt and Dr. Jörg Renkawitz for plasma coater access. Library preparation and sequencing were performed at the Helmholtz Zentrum München (HMGU) by the Genomics Core Facility (Dr. Gertrud Eckstein and Dr. Inti De la Rosa Velazquez). We acknowledge the technical support of Core Facility Genomics and Core Facility Bioinformatics and Statistics at Helmholtz Munich. We thank Dr. Thomas Walzthöni for help with the Galaxy workflow pipeline for RNA-seq data alignment and processing. We thank Dr. Julia Becker (Cambridge, PDN) for Sneddon model fitting in AFM experiments. We thank Dr. Maria Richter for suggestions on bioinformatic analysis. We thank Claire Malvezin for support in calcium exposure and 2D comparison assays. We would like to thank PD Dr. Swetlana Sirko for discussions on astrocyte biology and Dr. Yvette Zarb for critical discussion of the manuscript. This work was funded by the German Research Foundation TRR274 (no. 408885537 to M.G.), FOR2879/2 (no. 405358801 to M.G.), SyNergy (EXC2145/project-ID 390857198, M.G.), SPP2502 (no. 563470442 to G.M.), and CRC1540 EBM (project-ID 460333672 to K.F.), as well as the European Research Council (Synergy Grant 101118729 UNFOLD to K.F.) and an Alexander von Humboldt Professorship (Alexander von Humboldt Foundation to K.F.). This work was supported by the Impulse and Networking Fund of the Helmholtz Association (Helmholtz Excellence Network BioEM, grant EXNET-01-14) to M.G. and by a New Frontiers in Research Fund Transformation grant to M.G., funded through three Canadian federal funding agencies (CIHR, NSERC, and SSHRC) and the European Union's Horizon 2020 research and innovation program under grant agreement no. 874758 (NSC Reconstruct to M.G.).

AUTHOR CONTRIBUTIONS

Conceptualization, G.M., T.D., and M.G.; methodology, T.D. (hydrogels, 3D cell culture, and live imaging), T.D., G.M., M.G. (3D reprogramming), M.B., G.M. (iPSC-to-astrocytes differentiation), M.B. (virus production), S.V.-S., and K.F. (AFM); investigation, T.D., M.B. (reprogramming experiments), T.D., S.V.S. (AFM experiments), T.D., and K.K.D. (bulk RNA-seq experiments, proliferation, and viability assays); resources, K.F. and M.G.; formal analysis, T.D., K.K.D., S.V.-S., and G.M.; supervision, G.M. and M.G.; funding acquisition, K.F., M.G., and G.M.; writing, T.D., G.M., and M.G.; and all authors contributed corrections and comments.

DECLARATION OF INTERESTS

The authors declare no competing interests.

SUPPLEMENTAL INFORMATION

Supplemental information can be found online at https://doi.org/10.1016/j.celbio.2026.100493.

Received: November 6, 2025
Revised: March 9, 2026
Accepted: April 28, 2026

REFERENCES

1. Soto, J.S., and Khakh, B.S. (2023). Cell morphology: Astrocyte structure at the nanoscale. Curr. Biol. *33*, R200–R202. https://doi.org/10.1016/j.cub.2023.01.045.
2. Miller, S.J. (2018). Astrocyte Heterogeneity in the Adult Central Nervous System. Front. Cell. Neurosci. *12*, 401. https://doi.org/10.3389/fncel.2018.00401.
3. Escartin, C., Galea, E., Lakatos, A., O'Callaghan, J.P., Petzold, G.C., Serrano-Pozo, A., Steinhäuser, C., Volterra, A., Carmignoto, G., Agarwal, A., et al. (2021). Reactive astrocyte nomenclature, definitions, and future directions. Nat. Neurosci. *24*, 312–325. https://doi.org/10.1038/s41593-020-00783-4.
4. Sofroniew, M.V., and Vinters, H.V. (2010). Astrocytes: biology and pathology. Acta Neuropathol. *119*, 7–35. https://doi.org/10.1007/s00401-009-0619-8.
5. Patani, R., Hardingham, G.E., and Liddelow, S.A. (2023). Functional roles of reactive astrocytes in neuroinflammation and neurodegeneration. Nat. Rev. Neurol. *19*, 395–409. https://doi.org/10.1038/s41582-023-00822-1.
6. Anderson, M.A., Burda, J.E., Ren, Y., Ao, Y., O'Shea, T.M., Kawaguchi, R., Coppola, G., Khakh, B.S., Deming, T.J., and Sofroniew, M.V. (2016). Astrocyte scar formation AIDS central nervous system axon regeneration. Nature *532*, 195–200. https://doi.org/10.1038/nature17623.
7. Pekny, M., and Pekna, M. (2014). Astrocyte reactivity and reactive astrogliosis: Costs and benefits. Physiol. Rev. *94*, 1077–1098. https://doi.org/10.1152/physrev.00041.2013.
8. Verkhratsky, A., Butt, A., Li, B., Illes, P., Zorec, R., Semyanov, A., Tang, Y., and Sofroniew, M.V. (2023). Astrocytes in human central nervous system diseases: a frontier for new therapies. Signal Transduct. Target. Ther. *8*, 396. https://doi.org/10.1038/s41392-023-01628-9.
9. Bardehle, S., Krüger, M., Buggenthin, F., Schwausch, J., Ninkovic, J., Clevers, H., Snippert, H.J., Theis, F.J., Meyer-Luehmann, M., Bechmann, I., et al. (2013). Live imaging of astrocyte responses to acute injury reveals selective juxtavascular proliferation. Nat. Neurosci. *16*, 580–586. https://doi.org/10.1038/nn.3371.
10. Frik, J., Merl-Pham, J., Plesnila, N., Mattugini, N., Kjell, J., Kraska, J., Gómez, R.M., Hauck, S.M., Sirko, S., and Götz, M. (2018). Cross-talk between monocyte invasion and astrocyte proliferation regulates scarring in brain injury. EMBO Rep. *19*, e45294. https://doi.org/10.15252/embr.201745294.
11. Sirko, S., Behrendt, G., Johansson, P.A., Tripathi, P., Costa, M., Bek, S., Heinrich, C., Tiedt, S., Colak, D., Dichgans, M., et al. (2013). Reactive glia in the injured brain acquire stem cell properties in response to sonic hedgehog glia. Cell Stem Cell *12*, 426–439. https://doi.org/10.1016/j.stem.2013.01.019.
12. Liddelow, S.A., Guttenplan, K.A., Clarke, L.E., Bennett, F.C., Bohlen, C.J., Schirmer, L., Bennett, M.L., Münch, A.E., Chung, W.S., Peterson, T.C.,

Please cite this article in press as: Distler et al., Fibrin hydrogels regulate human astrocyte state and neuronal reprogramming, Cell Biomaterials (2026), https://doi.org/10.1016/j.celbio.2026.100493

et al. (2017). Neurotoxic reactive astrocytes are induced by activated microglia. Nature *541*, 481–487. https://doi.org/10.1038/nature21029.

13. Guttenplan, K.A., Weigel, M.K., Prakash, P., Wijewardhane, P.R., Hasel, P., Rufen-Blanchette, U., Münch, A.E., Blum, J.A., Fine, J., Neal, M.C., et al. (2021). Neurotoxic reactive astrocytes induce cell death via saturated lipids. Nature *599*, 102–107. https://doi.org/10.1038/s41586-021-03960-y.
14. Guttenplan, K.A., Stafford, B.K., El-Danaf, R.N., Adler, D.I., Münch, A.E., Weigel, M.K., Huberman, A.D., and Liddelow, S.A. (2020). Neurotoxic Reactive Astrocytes Drive Neuronal Death after Retinal Injury. Cell Rep. *31*, 107776. https://doi.org/10.1016/j.celrep.2020.107776.
15. Conforti, P., Mezey, S., Nath, S., Chu, Y.H., Malik, S.C., Martínez Santamaría, J.C., Deshpande, S.S., Pous, L., Zieger, B., and Schachtrup, C. (2022). Fibrinogen regulates lesion border-forming reactive astrocyte properties after vascular damage. Glia *70*, 1251–1266. https://doi.org/10.1002/glia.24166.
16. Nahon, D.M., Vila Cuenca, M., van den Hil, F.E., Hu, M., de Korte, T., Frimat, J.P., van den Maagdenberg, A.M.J.M., Mummery, C.L., and Orlova, V.V. (2024). Self-assembling 3D vessel-on-chip model with hiPSC-derived astrocytes. Stem Cell Rep. *19*, 946–956. https://doi.org/10.1016/j.stemcr.2024.05.006.
17. Campisi, M., Shin, Y., Osaki, T., Hajal, C., Chiono, V., and Kamm, R.D. (2018). 3D self-organized microvascular model of the human blood-brain barrier with endothelial cells, pericytes and astrocytes. Biomaterials *180*, 117–129. https://doi.org/10.1016/j.biomaterials.2018.07.014.
18. Santos, R., Vadodaria, K.C., Jaeger, B.N., Mei, A., Lefcochilos-Fogelquist, S., Mendes, A.P.D., Erikson, G., Shokhirev, M., Randolph-Moore, L., Fredlender, C., et al. (2017). Differentiation of Inflammation-Responsive Astrocytes from Glial Progenitors Generated from Human Induced Pluripotent Stem Cells. Stem Cell Rep. *8*, 1757–1769. https://doi.org/10.1016/j.stemcr.2017.05.011.
19. Sonsalla, G., Malpartida, A.B., Riedemann, T., Gusic, M., Rusha, E., Bulli, G., Najas, S., Janjic, A., Hersbach, B.A., Smialowski, P., et al. (2024). Direct neuronal reprogramming of NDUFS4 patient cells identifies the unfolded protein response as a novel general reprogramming hurdle. Neuron *112*, 1117–1132.e9. https://doi.org/10.1016/j.neuron.2023.12.020.
20. O'Shea, T.M., Ao, Y., Wang, S., Ren, Y., Cheng, A.L., Kawaguchi, R., Shi, Z., Swarup, V., and Sofroniew, M.V. (2024). Derivation and transcriptional reprogramming of border-forming wound repair astrocytes after spinal cord injury or stroke in mice. Nat. Neurosci. *27*, 1505–1521. https://doi.org/10.1038/s41593-024-01684-6.
21. Magnusson, J.P., Zamboni, M., Santopolo, G., Mold, J.E., Barrientos-Somarribas, M., Talavera-Lopez, C., Andersson, B., and Frisén, J. (2020). Activation of a neural stem cell transcriptional program in parenchymal astrocytes. eLife *9*, e59733. https://doi.org/10.7554/ELIFE.59733.
22. Gascón, S., Murenu, E., Masserdotti, G., Ortega, F., Russo, G.L., Petrik, D., Deshpande, A., Heinrich, C., Karow, M., Robertson, S.P., et al. (2016). Identification and Successful Negotiation of a Metabolic Checkpoint in Direct Neuronal Reprogramming. Cell Stem Cell *18*, 396–409. https://doi.org/10.1016/j.stem.2015.12.003.
23. Sirko, S., Schichor, C., Della Vecchia, P., Metzger, F., Sonsalla, G., Simon, T., Bürkle, M., Kalpazidou, S., Ninkovic, J., Masserdotti, G., et al. (2023). Injury-specific factors in the cerebrospinal fluid regulate astrocyte plasticity in the human brain. Nat. Med. *29*, 3149–3161. https://doi.org/10.1038/s41591-023-02644-6.
24. Galarza, S., Crosby, A.J., Pak, C.H., and Peyton, S.R. (2020). Control of Astrocyte Quiescence and Activation in a Synthetic Brain Hydrogel. Adv. Healthc. Mater. *9*, e1901419. https://doi.org/10.1002/adhm.201901419.
25. Gailit, J., Clarke, C., Newman, D., Tonnesen, M.G., Mosesson, M.W., and Clark, R.A.F. (1997). Human Fibroblasts Bind Directly to Fibrinogen at RGD Sites through Integrin alphavbeta3. Exp. Cell Res. *232*, 118–126. https://doi.org/10.1006/excr.1997.3512.
26. Mosesson, M.W. (2003). Fibrinogen γ chain functions. J. Thromb. Haemost. *1*, 231–238. https://doi.org/10.1046/j.1538-7836.2003.00063.x.
27. Thiagarajan, P., Rippon, A.J., and Farrell, D.H. (1996). Alternative Adhesion Sites in Human Fibrinogen for Vascular Endothelial Cells. Biochemistry *35*, 4169–4175. https://doi.org/10.1021/bi952532b.
28. Millesi, F., Mero, S., Semmler, L., Rad, A., Stadlmayr, S., Borger, A., Supper, P., Haertinger, M., Ploszczanski, L., Windberger, U., et al. (2023). Systematic Comparison of Commercial Hydrogels Revealed That a Synergy of Laminin and Strain-Stiffening Promotes Directed Migration of Neural Cells. ACS Appl. Mater. Interfaces *15*, 12678–12695. https://doi.org/10.1021/acsami.2c20040.
29. Caliari, S.R., and Burdick, J.A. (2016). A practical guide to hydrogels for cell culture. Nat. Methods *13*, 405–414. https://doi.org/10.1038/nmeth.3839.
30. Lattke, M., Goldstone, R., Ellis, J.K., Boeing, S., Jurado-Arjona, J., Marichal, N., MacRae, J.I., Berninger, B., and Guillemot, F. (2021). Extensive transcriptional and chromatin changes underlie astrocyte maturation in vivo and in culture. Nat. Commun. *12*, 4335. https://doi.org/10.1038/s41467-021-24624-5.
31. Segel, M., Neumann, B., Hill, M.F.E., Weber, I.P., Viscomi, C., Zhao, C., Young, A., Agley, C.C., Thompson, A.J., Gonzalez, G.A., et al. (2019). Niche stiffness underlies the ageing of central nervous system progenitor cells. Nature *573*, 130–134. https://doi.org/10.1038/s41586-019-1484-9.
32. Miroshnikova, Y.A., Mouw, J.K., Barnes, J.M., Pickup, M.W., Lakins, J.N., Kim, Y., Lobo, K., Persson, A.I., Reis, G.F., McKnight, T.R., et al. (2016). Tissue mechanics promote IDH1-dependent HIF1α-tenascin C feedback to regulate glioblastoma aggression. Nat. Cell Biol. *18*, 1336–1345. https://doi.org/10.1038/ncb3429.
33. Schmitt, A., Rödel, P., Anamur, C., Seeliger, C., Imhoff, A.B., Herbst, E., Vogt, S., Van Griensven, M., Winter, G., and Engert, J. (2015). Calcium alginate gels as stem cell matrix -making paracrine stem cell activity available for enhanced healing after surgery. PLoS One *10*, e0118937. https://doi.org/10.1371/journal.pone.0118937.
34. Matyash, M., Despang, F., Ikonomidou, C., and Gelinsky, M. (2014). Swelling and mechanical properties of alginate hydrogels with respect to promotion of neural growth. Tissue Eng. Part C Methods *20*, 401–411. https://doi.org/10.1089/ten.tec.2013.0252.
35. Tekin, H., Simmons, S., Cummings, B., Gao, L., Adiconis, X., Hession, C.C., Ghoshal, A., Dionne, D., Choudhury, S.R., Yesilyurt, V., et al. (2018). Effects of 3D culturing conditions on the transcriptomic profile of stem-cell-derived neurons. Nat. Biomed. Eng. *2*, 540–554. https://doi.org/10.1038/s41551-018-0219-9.
36. Salsmann, A., Schaffner-Reckinger, E., Kabile, F., Plançon, S., and Kieffer, N. (2005). A new functional role of the fibrinogen RGD motif as the molecular switch that selectively triggers integrin αIIbβ3-dependent RhoA activation during cell spreading. J. Biol. Chem. *280*, 33610–33619. https://doi.org/10.1074/jbc.M500146200.
37. Gorodetsky, R., Vexler, A., Shamir, M., An, J., Levdansky, L., Shimeliovich, I., and Marx, G. (2003). New cell attachment peptide sequences from conserved epitopes in the carboxy termini of fibrinogen. Exp. Cell Res. *287*, 116–129. https://doi.org/10.1016/S0014-4827(03)00120-4.
38. Reyhani, V., Seddigh, P., Guss, B., Gustafsson, R., Rask, L., and Rubin, K. (2014). Fibrin binds to collagen and provides a bridge for αVβ3 integrin-dependent contraction of collagen gels. Biochem. J. *462*, 113–123. https://doi.org/10.1042/BJ20140201.
39. Bocchi, R., Thorwirth, M., Simon-Ebert, T., Koupourtidou, C., Clavreul, S., Kolf, K., Della Vecchia, P., Bottes, S., Jessberger, S., Zhou, J., et al. (2025). Astrocyte heterogeneity reveals region-specific astrogenesis in the white matter. Nat. Neurosci. *28*, 457–469. https://doi.org/10.1038/s41593-025-01878-6.
40. Song, Y., Jiang, W., Afridi, S.K., Wang, T., Zhu, F., Xu, H., Nazir, F.H., Liu, C., Wang, Y., Long, Y., et al. (2024). Astrocyte-derived CHI3L1 signaling impairs neurogenesis and cognition in the demyelinated hippocampus. Cell Rep. *43*, 114226. https://doi.org/10.1016/j.celrep.2024.114226.
41. Zhang, Y., Sloan, S.A., Clarke, L.E., Caneda, C., Plaza, C.A., Blumenthal, P.D., Vogel, H., Steinberg, G.K., Edwards, M.S.B., Li, G., et al. (2016).

Purification and Characterization of Progenitor and Mature Human Astrocytes Reveals Transcriptional and Functional Differences with Mouse. Neuron *89*, 37–53. https://doi.org/10.1016/j.neuron.2015.11.013.

42. Barbar, L., Jain, T., Zimmer, M., Kruglikov, I., Sadick, J.S., Wang, M., Kalpana, K., Rose, I.V.L., Burstein, S.R., Rusielewicz, T., et al. (2020). CD49f Is a Novel Marker of Functional and Reactive Human iPSC-Derived Astrocytes. Neuron *107*, 436–453.e12. https://doi.org/10.1016/j.neuron.2020.05.014.
43. Sadick, J.S., O'Dea, M.R., Hasel, P., Dykstra, T., Faustin, A., and Liddelow, S.A. (2022). Astrocytes and oligodendrocytes undergo subtype-specific transcriptional changes in Alzheimer's disease. Neuron *110*, 1788–1805.e10. https://doi.org/10.1016/j.neuron.2022.03.008.
44. Bormann, D., Knoflach, M., Poreba, E., Riedl, C.J., Testa, G., Orset, C., Levilly, A., Cottereau, A., Jauk, P., Hametner, S., et al. (2024). Single-nucleus RNA sequencing reveals glial cell type-specific responses to ischemic stroke in male rodents. Nat. Commun. *15*, 6232. https://doi.org/10.1038/s41467-024-50465-z.
45. Rempe, R.G., Hartz, A.M.S., and Bauer, B. (2016). Matrix metalloproteinases in the brain and blood-brain barrier: Versatile breakers and makers. J. Cereb. Blood Flow Metab. *36*, 1481–1507. https://doi.org/10.1177/0271678X16655551.
46. Liu, Y., Zhang, M., Hao, W., Mihaljevic, I., Liu, X., Xie, K., Walter, S., and Fassbender, K. (2013). Matrix metalloproteinase-12 contributes to neuroinflammation in the aged brain. Neurobiol. Aging *34*, 1231–1239. https://doi.org/10.1016/j.neurobiolaging.2012.10.015.
47. Wang, P., Gorter, R.P., de Jonge, J.C., Nazmuddin, M., Zhao, C., Amor, S., Hoekstra, D., and Baron, W. (2018). MMP7 cleaves remyelination-impairing fibronectin aggregates and its expression is reduced in chronic multiple sclerosis lesions. Glia *66*, 1625–1643. https://doi.org/10.1002/glia.23328.
48. Shibasaki, K., Ikenaka, K., Tamalu, F., Tominaga, M., and Ishizaki, Y. (2014). A novel subtype of astrocytes expressing TRPV4 (Transient Receptor Potential Vanilloid 4) Regulates neuronal excitability via release of gliotransmitters. J. Biol. Chem. *289*, 14470–14480. https://doi.org/10.1074/jbc.M114.557132.
49. Morales-Lázaro, S.L., Lemus, L., and Rosenbaum, T. (2017). Regulation of thermoTRPs by lipids. Temperature *4*, 24–40. https://doi.org/10.1080/23328940.2016.1254136.
50. Benfenati, V., Caprini, M., Dovizio, M., Mylonakou, M.N., Ferroni, S., Ottersen, O.P., and Amiry-Moghaddam, M. (2011). An aquaporin-4/transient receptor potential vanilloid 4 (AQP4/TRPV4) complex is essential for cell-volume control in astrocytes. Proc. Natl. Acad. Sci. USA *108*, 2563–2568. https://doi.org/10.1073/pnas.1012867108.
51. Robel, S., Bardehle, S., Lepier, A., Brakebusch, C., and Götz, M. (2011). Genetic deletion of Cdc42 reveals a crucial role for astrocyte recruitment to the injury site in vitro and in vivo. J. Neurosci. *31*, 12471–12482. https://doi.org/10.1523/JNEUROSCI.2696-11.2011.
52. Puglisi, M., Lao, C.L., Wani, G., Masserdotti, G., Bocchi, R., and Götz, M. (2024). Comparing Viral Vectors and Fate Mapping Approaches for Astrocyte-to-Neuron Reprogramming in the Injured Mouse Cerebral Cortex. Cells *13*, 1408. https://doi.org/10.3390/cells13171408.
53. Hand, R., Bortone, D., Mattar, P., Nguyen, L., Heng, J.I.T., Guerrier, S., Boutt, E., Peters, E., Barnes, A.P., Parras, C., et al. (2005). Phosphorylation of neurogenin2 specifies the migration properties and the dendritic morphology of pyramidal neurons in the neocortex. Neuron *48*, 45–62. https://doi.org/10.1016/j.neuron.2005.08.032.
54. Ali, F., Hindley, C., McDowell, G., Deibler, R., Jones, A., Kirschner, M., Guillemot, F., and Philpott, A. (2011). Cell cycle-regulated multi-site phosphorylation of neurogenin 2 coordinates cell cycling with differentiation during neurogenesis. Development *138*, 4267–4277. https://doi.org/10.1242/dev.067900.
55. Hindley, C., Ali, F., McDowell, G., Cheng, K., Jones, A., Guillemot, F., and Philpott, A. (2012). Post-translational modification of Ngn2 differentially affects transcription of distinct targets to regulate the balance between progenitor maintenance and differentiation. Development *139*, 1718–1723. https://doi.org/10.1242/dev.077552.
56. Pereira, A., Diwakar, J., Masserdotti, G., Beşkardeş, S., Simon, T., So, Y., Martín-Loarte, L., Bergemann, F., Vasan, L., Schauer, T., et al. (2024). Direct neuronal reprogramming of mouse astrocytes is associated with multiscale epigenome remodeling and requires Yy1. Nat. Neurosci. *27*, 1260–1273. https://doi.org/10.1038/s41593-024-01677-5.
57. Budday, S., Sommer, G., Birkl, C., Langkammer, C., Haybaeck, J., Kohnert, J., Bauer, M., Paulsen, F., Steinmann, P., Kuhl, E., et al. (2017). Mechanical characterization of human brain tissue. Acta Biomater. *48*, 319–340. https://doi.org/10.1016/j.actbio.2016.10.036.
58. Baek, J., Lopez, P.A., Lee, S., Kim, T.-S., Kumar, S., and Schaffer, D.V. (2022). Egr1 is a 3D matrix-specific mediator of mechanosensitive stem cell lineage commitment. Sci. Adv. *8*, eabm4646. https://doi.org/10.1126/sciadv.abm4646.
59. Martínez, G.F., Fagetti, J., Vierci, G., Brauer, M.M., Unsain, N., and Richeri, A. (2022). Extracellular matrix stiffness negatively affects axon elongation, growth cone area and F-actin levels in a collagen type I 3D culture. J. Tissue Eng. Regen. Med. *16*, 151–162. https://doi.org/10.1002/term.3269.
60. Lampe, K.J., Antaris, A.L., and Heilshorn, S.C. (2013). Design of three-dimensional engineered protein hydrogels for tailored control of neurite growth. Acta Biomater. *9*, 5590–5599. https://doi.org/10.1016/j.actbio.2012.10.033.
61. Budday, S., Nay, R., de Rooij, R., Steinmann, P., Wyrobek, T., Ovaert, T.C., and Kuhl, E. (2015). Mechanical properties of gray and white matter brain tissue by indentation. J. Mech. Behav. Biomed. Mater. *46*, 318–330. https://doi.org/10.1016/j.jmbbm.2015.02.024.
62. Wang, M., Zhang, L., Novak, S.W., Yu, J., Gallina, I.S., Xu, L.L., Lim, C.K., Fernandes, S., Shokhirev, M.N., Williams, A.E., et al. (2024). Morphological diversification and functional maturation of human astrocytes in glia-enriched cortical organoid transplanted in mouse brain. Nat. Biotechnol. *43*, 52–62. https://doi.org/10.1038/s41587-024-02157-8.
63. Hajal, C., Offeddu, G.S., Shin, Y., Zhang, S., Morozova, O., Hickman, D., Knutson, C.G., and Kamm, R.D. (2022). Engineered human blood–brain barrier microfluidic model for vascular permeability analyses. Nat. Protoc. *17*, 95–128. https://doi.org/10.1038/s41596-021-00635-w.
64. Yao, L., Sai, H.V., Shippy, T., and Li, B. (2024). Cellular and Transcriptional Response of Human Astrocytes to Hybrid Protein Materials. ACS Appl. Bio Mater. *7*, 2887–2898. https://doi.org/10.1021/acsabm.3c01266.
65. Budday, S., Ovaert, T.C., Holzapfel, G.A., Steinmann, P., and Kuhl, E. (2019). Fifty Shades of Brain: A Review on the Mechanical Testing and Modeling of Brain Tissue. Arch. Comput. Methods Eng. *27*, 1187–1230. https://doi.org/10.1007/s11831-019-09352-w.
66. C Benincasa, J., Madias, M.I., Kandell, R.M., Delgado-Garcia, L.M., Engler, A.J., Kwon, E.J., and Porcionatto, M.A. (2024). Mechanobiological Modulation of In Vitro Astrocyte Reactivity Using Variable Gel Stiffness. ACS Biomater. Sci. Eng. *10*, 4279–4296. https://doi.org/10.1021/acsbiomaterials.4c00229.
67. Xiang, R., Wang, J., Chen, Z., Tao, J., Peng, Q., Ding, R., Zhou, T., Tu, Z., Wang, S., Yang, T., et al. (2025). Spatiotemporal transcriptomic maps of mouse intracerebral hemorrhage at single-cell resolution. Neuron *113*, 2102–2122.e7. https://doi.org/10.1016/j.neuron.2025.04.026.
68. Henrik Heiland, D., Ravi, V.M., Behringer, S.P., Frenking, J.H., Wurm, J., Joseph, K., Garrelfs, N.W.C., Strähle, J., Heynckes, S., Grauvogel, J., et al. (2019). Tumor-associated reactive astrocytes aid the evolution of immunosuppressive environment in glioblastoma. Nat. Commun. *10*, 2541. https://doi.org/10.1038/s41467-019-10493-6.
69. Barbar, L., Rusielewicz, T., Zimmer, M., Kalpana, K., and Fossati, V. (2020). Isolation of Human CD49f+ Astrocytes and In Vitro iPSC-Based Neurotoxicity Assays. STAR Protoc. *1*, 100172. https://doi.org/10.1016/j.xpro.2020.100172.

Please cite this article in press as: Distler et al., Fibrin hydrogels regulate human astrocyte state and neuronal reprogramming, Cell Biomaterials (2026), https://doi.org/10.1016/j.celbio.2026.100493

70. Koupourtidou, C., Schwarz, V., Aliee, H., Frerich, S., Fischer-Sternjak, J., Bocchi, R., Simon-Ebert, T., Bai, X., Sirko, S., Kirchhoff, F., et al. (2024). Shared inflammatory glial cell signature after stab wound injury, revealed by spatial, temporal, and cell-type-specific profiling of the murine cerebral cortex. Nat. Commun. *15*, 2866. https://doi.org/10.1038/s41467-024-46625-w.

71. Moeendarbary, E., Weber, I.P., Sheridan, G.K., Koser, D.E., Soleman, S., Haenzi, B., Bradbury, E.J., Fawcett, J., and Franze, K. (2017). The soft mechanical signature of glial scars in the central nervous system. Nat. Commun. *8*, 14787. https://doi.org/10.1038/ncomms14787.

72. Kajtez, J., Laurin, K., Nilsson, F., Bruzelius, A., Cepeda-Prado, E., Birtele, M., Barker, R.A., Herborg, F., Rylander Ottosson, D., Storm, P., et al. (2025). Three-dimensional cell-cell interactions promote direct reprogramming of patient fibroblasts into functional and transplantable neurons. Sci. Adv. *11*, eadq7855. https://doi.org/10.1126/sciadv.adq7855.

73. Jin, Y., Lee, J.S., Kim, J., Min, S., Wi, S., Yu, J.H., Chang, G.-E., Cho, A.-N., Choi, Y., Ahn, D.-H., et al. (2018). Three-dimensional brain-like microenvironments facilitate the direct reprogramming of fibroblasts into therapeutic neurons. Nat. Biomed. Eng. *2*, 522–539. https://doi.org/10.1038/s41551-018-0260-8.

74. Sun, Z., Kwon, J.S., Ren, Y., Chen, S., Walker, C.K., Lu, X., Cates, K., Karahan, H., Sviben, S., Fitzpatrick, J.A.J., et al. (2024). Modeling late-onset Alzheimer's disease neuropathology via direct neuronal reprogramming. Science *385*, adl2992. https://doi.org/10.1126/science.adl2992.

75. Giacomoni, J., Bruzelius, A., Habekost, M., Kajtez, J., Ottosson, D.R., Fiorenzano, A., Storm, P., and Parmar, M. (2024). 3D model for human glia conversion into subtype-specific neurons, including dopamine neurons. Cell Rep. Methods *4*, 100845. https://doi.org/10.1016/j.crmeth.2024.100845.

76. Götz, M., Sirko, S., Beckers, J., and Irmler, M. (2015). Reactive astrocytes as neural stem or progenitor cells: In vivo lineage, In vitro potential, and Genome-wide expression analysis. Glia *63*, 1452–1468. https://doi.org/10.1002/glia.22850.

77. LeSavage, B.L., Suhar, N.A., Madl, C.M., and Heilshorn, S.C. (2018). Production of Elastin-like Protein Hydrogels for Encapsulation and Immunostaining of Cells in 3D. J. Vis. Exp. 57739. https://doi.org/10.3791/57739.

78. Vorwald, C.E., Gonzalez-Fernandez, T., Joshee, S., Sikorski, P., and Leach, J.K. (2020). Tunable fibrin-alginate interpenetrating network hydrogels to support cell spreading and network formation. Acta Biomater. *108*, 142–152. https://doi.org/10.1016/j.actbio.2020.03.014.

79. Hutter, J.L., and Bechhoefer, J. (1993). Calibration of atomic-force microscope tips. Rev. Sci. Instrum. *64*, 1868–1873. https://doi.org/10.1063/1.1143970.

80. Schindelin, J., Arganda-Carreras, I., Frise, E., Kaynig, V., Longair, M., Pietzsch, T., Preibisch, S., Rueden, C., Saalfeld, S., Schmid, B., et al. (2012). Fiji: An open-source platform for biological-image analysis. Nat. Methods *9*, 676–682. https://doi.org/10.1038/nmeth.2019.

81. Feng, L., Zhao, T., and Kim, J. (2015). Neutube 1.0: A new design for efficient neuron reconstruction software based on the swc format. eNeuro *2*, ENEURO.0049-14.2014. https://doi.org/10.1523/ENEURO.0049-14.2014.

82. Arshadi, C., Günther, U., Eddison, M., Harrington, K.I.S., and Ferreira, T.A. (2021). SNT: a unifying toolbox for quantification of neuronal anatomy. Nat. Methods *18*, 374–377. https://doi.org/10.1038/s41592-021-01105-7.

83. Bolger, A.M., Lohse, M., and Usadel, B. (2014). Trimmomatic: A flexible trimmer for Illumina sequence data. Bioinformatics *30*, 2114–2120. https://doi.org/10.1093/bioinformatics/btu170.

84. Genome Reference Consortium (2019). Genome Reference Consortium Human Build 38 patch release 13 (GRCh38.p13). https://doi.org/https://www.gencodegenes.org/human/release_32.html.

85. Alexa, A., and Rahnenfuhrer, J. (2025). topGO: Enrichment Analysis for Gene Ontology. Bioconductor. https://doi.org/10.18129/B9.bioc.topGO.

86. Korotkevich, G., Sukhov, V., Budin, N., Shpak, B., Artyomov, M.N., and Sergushichev, A. (2019). Fast gene set enrichment analysis. Preprint at bioRxiv. https://doi.org/10.1101/060012.

87. Heinrich, C., Blum, R., Gascón, S., Masserdotti, G., Tripathi, P., Sánchez, R., Tiedt, S., Schroeder, T., Götz, M., and Berninger, B. (2010). Directing astroglia from the cerebral cortex into subtype specific functional neurons. PLoS Biol. *8*, e1000373. https://doi.org/10.1371/journal.pbio.1000373.

88. Heinrich, C., Gascón, S., Masserdotti, G., Lepier, A., Sanchez, R., Simon-Ebert, T., Schroeder, T., Götz, M., and Berninger, B. (2011). Generation of subtype-specific neurons from postnatal astroglia of the mouse cerebral cortex. Nat. Protoc. *6*, 214–228. https://doi.org/10.1038/nprot.2010.188.

89. Drouin-Ouellet, J., Lau, S., Brattås, P.L., Rylander Ottosson, D., Pircs, K., Grassi, D.A., Collins, L.M., Vuono, R., Andersson Sjöland, A., Westergren-Thorsson, G., et al. (2017). REST suppression mediates neural conversion of adult human fibroblasts via microRNA-dependent and -independent pathways. EMBO Mol. Med. *9*, 1117–1131. https://doi.org/10.15252/emmm.201607471.

90. Love, M.I., Huber, W., and Anders, S. (2014). Moderated estimation of fold change and dispersion for RNA-seq data with DESeq2. Genome Biol. *15*, 550. https://doi.org/10.1186/s13059-014-0550-8.

91. Wickham, H. (2016). ggplot2 – Elegant Graphics for Data Analysis (Springer-Verlag). Second Edition.